Regional Global Navigation Satellite System Networks for Crustal Deformation Monitoring

Jessica R. Murray*[1], Noel Bartlow[2], Yehuda Bock[3], Benjamin A. Brooks[1], James Foster[4], Jeffrey Freymueller[5], William C. Hammond[6], Kathleen Hodgkinson[7], Ingrid Johanson[8], Alberto López-Venegas[9], Dörte Mann[7], Glen S. Mattioli[7], Timothy Melbourne[10], David Mencin[7], Emily Montgomery-Brown[1], Mark H. Murray[1], Robert Smalley[11], and Valerie Thomas[12]

Abstract

Regional networks of Global Navigation Satellite System (GNSS) stations cover seismically and volcanically active areas throughout the United States. Data from these networks have been used to produce high-precision, three-component velocity fields covering broad geographic regions as well as position time series that track time-varying crustal deformation. This information has contributed to assessing interseismic strain accumulation and related seismic hazard, revealed previously unknown occurrences of aseismic fault slip, constrained coseismic slip estimates, and enabled monitoring of volcanic unrest and postseismic deformation. In addition, real-time GNSS data are now widely available. Such observations proved invaluable for tracking the rapidly evolving eruption of Kīlauea in 2018. Real-time earthquake source modeling using GNSS data is being incorporated into tsunami warning systems, and a vigorous research effort is focused on quantifying the contribution that real-time GNSS can make to improve earthquake early warnings as part of the Advanced National Seismic System ShakeAlert system. Real-time GNSS data can also aid in the tracking of ionospheric disturbances and precipitable water vapor for weather forecasting. Although regional GNSS and seismic networks generally have been established independently, their spatial footprints often overlap, and in some cases the same institution operates both types of networks. Further integration of GNSS and seismic networks would promote joint use of the two data types to better characterize earthquake sources and ground motion as well as offer opportunities for more efficient network operations. Looking ahead, upgrading network stations to leverage new GNSS technology could enable more precise positioning and robust real-time operations. New computational approaches such as machine learning have the potential to enable full utilization of the large amounts of data generated by continuous GNSS networks. Development of seafloor Global Positioning System-acoustic networks would provide unique information for fundamental and applied research on subduction zone seismic hazard and, potentially, monitoring.

Cite this article as Murray, J. R., N. Bartlow, Y. Bock, B. A. Brooks, J. Foster, J. Freymueller, W. C. Hammond, K. Hodgkinson, I. Johanson, A. López-Venegas, *et al.* (2019). Regional Global Navigation Satellite System Networks for Crustal Deformation Monitoring, *Seismol. Res. Lett.* **91**, 552–572, doi: 10.1785/0220190113.

Introduction

Global Navigation Satellite Systems (GNSSs), of which the Global Positioning System (GPS) is an example, are a major source of data for geophysical applications. The precise 3D coordinates calculated from data collected during repeated GNSS measurements record the motion of geodetic benchmarks on the Earth's surface. These data directly measure arbitrarily large displacements as might occur during earthquakes or volcanic eruptions, but they also resolve crustal motion at the millimeter-per-year level over continental scales. Furthermore, GNSS enables observation of deformation processes that do not release significant seismic energy and thus, for which seismic data

1. U.S. Geological Survey, Menlo Park, California, U.S.A.; 2. Seismological Laboratory, University of California, Berkeley, Berkeley, California, U.S.A.; 3. Scripps Institution of Oceanography, Institute of Geophysics and Planetary Physics, University of California San Diego, La Jolla, California, U.S.A.; 4. Hawai'i Institute of Geophysics and Planetology, University of Hawai'i at Mānoa, Honolulu, Hawaii, U.S.A.; 5. Department of Earth and Environmental Sciences, Michigan State University, East Lansing, Michigan, U.S.A.; 6. Nevada Geodetic Laboratory, Nevada Bureau of Mines and Geology, University of Nevada, Reno, Reno, Nevada, U.S.A.; 7. UNAVCO, Inc., Boulder, Colorado, U.S.A.; 8. Hawaiian Volcano Observatory, U.S. Geological Survey, Hilo, Hawai'i, U.S.A.; 9. Department of Geology, University of Puerto Rico, Mayagüez, Puerto Rico, U.S.A.; 10. Department of Geological Sciences, Central Washington University, Ellensburg, Washington, U.S.A.; 11. Center for Earthquake Research and Information, The University of Memphis, Memphis, Tennessee, U.S.A.; 12. U.S. Geological Survey, Pasadena, California, U.S.A.

*Corresponding author: jrmurray@usgs.gov

provide limited information. Examples include interseismic strain, magma migration, earthquake afterslip, postseismic relaxation, glacial isostatic adjustment, and slow fault-slip events.

In the mid-1980s, GPS began to replace older geodetic methods, such as trilateration and leveling, for measuring crustal deformation (e.g., Dixon, 1991). Two trends shaped the development of GNSS networks since then: the transition to continuous operation and the expansion from locally focused station arrays to large-areal spatial coverage.

Initially, GPS surveys followed the approach of data collection via temporary, campaign-style field deployments, sometimes at the same benchmark networks previously observed with older methods. Repeat surveys of a given network were often separated by several years. Although the average velocities of measurement sites over years to decades can be estimated from GNSS data collected during infrequent campaign surveys, many deformation processes exhibit temporal variations that can only be observed with continuously recorded data (Segall and Davis, 1997; Bürgmann and Thatcher, 2013; Bock and Melgar, 2016). For example, detecting strain transients was one objective of the Southern California Integrated GPS Network (SCIGN, established in 1994; Hudnut *et al.*, 2002), one of the early United States (U.S.) continuously recording, permanently installed GPS (continuous GPS [cGPS]) networks. Events such as the 1994 M_w 6.7 Northridge earthquake and ongoing unrest at several North American volcanoes further motivated the push to establish cGPS networks throughout the western U.S. This effort accelerated in the mid-1990s, capitalizing on the increasing affordability of GPS instrumentation. Installation of the Plate Boundary Observatory (PBO) between 2003 and 2008 expanded the scope of these networks significantly. In parallel, a vast network of semicontinuous GPS (scGPS) sites was built in the Basin and Range (Blewitt *et al.*, 2009).

In most cases, U.S. cGPS networks were established independently of regional seismic networks with spatial distributions driven by the geodetic detectability of deformation processes. However, the two types of networks often cover similar geographic areas and in some regions are operated by the same institutions. Opportunities for joint use of seismic and geodetic data (e.g., Bock *et al.*, 2011), along with efficiencies possible through shared infrastructure, motivate the greater integration of geodetic and seismic network operations and collocation of instrumentation. The Advanced National Seismic System (ANSS) strategic plan (U.S. Geological Survey [USGS], 2017) cites the incorporation of real-time geodetic data into ANSS products and inclusion of geodetic networks as full ANSS participants as an opportunity for improving earthquake early warning (EEW) and rapid impact assessment following natural disasters. Indeed, several GNSS networks already receive partial ANSS support through the build-out of the west coast EEW system, ShakeAlert, and through cooperative agreements for geodetic network operations.

In this article, we discuss the ways in which these networks are leveraging modern GNSS technology, real-time data processing strategies, and integration with regional seismic networks to provide robust and timely observations for research and natural hazard applications. We also consider innovations such as seafloor geodetic methods and the application of machine learning (ML) to geoscience problems that inspire future directions for regional GNSS networks and the activities they support.

Background on GNSS

GNSS satellites transmit signals at multiple frequencies in the L-band (1–2 GHz) that are recorded by ground-based receivers paired with GNSS antennas. The signal travel times between at least four satellites and a ground station are used to determine the precise, 3D (i.e., east, north, and vertical) location of the antenna phase center via processing methods that employ models for satellite orbits, atmospheric signal delay, solid Earth tides, antenna phase center variations, and other factors. Position bias due to satellite clock drift is addressed by jointly processing data from a regional network of stations (Herring *et al.*, 2015) or by applying clock corrections determined independently using regional or global networks (Zumberge *et al.*, 1997). See Bock and Melgar (2016), Herring *et al.* (2016), and references therein for additional background. Although single-frequency signals are useful for some geophysical applications, use of dual-frequency signals enables the removal of first-order ionospheric delay and is the standard approach for high-precision positioning. The GPS constellation has been the primary source of data for U.S. networks. However, analyzing observations from multiple satellite systems (e.g., the European Union's Galileo, Russia's Global Navigation Satellite System (GLONASS), and China's BeiDou) can improve position accuracy, particularly for real-time high-rate (defined here as ≥1 Hz sampling) applications (Geng *et al.*, 2018). In this article, we use the more general term GNSS to indicate GPS and/or multiconstellation GNSS; we use GPS to indicate that only GPS signals are recorded or used.

The majority of the networks discussed here (Table 1) consist of permanently installed, continuously operating GNSS stations (cGNSS). A station includes a GNSS receiver and antenna along with power and data transmission systems (Fig. 1). Although these networks use a diverse collection of receiver and antenna models, all provide, at minimum, dual-frequency GPS signal tracking to allow for precise positioning with millimeter-level horizontal repeatability. Antennas are designed to minimize multipath (when the GNSS signal bounces off surrounding surfaces before reaching the antenna). Modern GNSS instrumentation supports multiple satellite constellations; because networks gradually upgrade their equipment, the availability of multi-GNSS data is expanding. In parallel, processing software is being extended to enable simultaneous analysis of multi-GNSS observables (Herring *et al.*, 2016).

TABLE 1
Description of Regional GNSS* Networks Discussed in this Article (See Data and Resources for Network and Archive Websites URLs)

Name	Acronym	Geographic Region	Year Established	Current Number of Stations	Number of Stations within 1.5 km of Seismic Station	Primary Institution for Operations and Maintenance	Data Archive	Notes
Alaska Deformation Array	AKDA	Alaska	1996	13	4	University of Alaska Fairbanks	UNAVCO	
Alaska Volcano Observatory	AVO	Alaska	2002	20	20	USGS VHP†, University of Alaska Fairbanks	UNAVCO	
Bay Area Regional Deformation network	BARD	Northern California	1992	33	24	University of California, Berkeley	NCEDC‡	
California Volcano Observatory Long Valley Network	CalVO	Volcanically active areas of California	1994	16	9	USGS VHP	UNAVCO	
Cascades Volcano Observatory	CVO	Cascades volcanoes	1997	31	18	USGS VHP	UNAVCO	
GPS Array for Mid-America	GAMA	New Madrid seismic zone	1997	16	4	University of Memphis	UNAVCO	
Hawaiian Volcano Observatory	HVO	Island of Hawai'i	1995	49	22	USGS VHP	UNAVCO	Additional nine stations are collocated with only tilt, gas, or gravity instruments
Mobile Array of GPS for Nevada Transtension	MAGNET	Basin and Range	2004	414	3	University of Nevada, Reno	UNAVCO	
Northern California GNSS Network	NCGN	Northern and central California	2010	9	3	USGS EHP§	NCEDC	

COCONet, Continuously Operating Caribbean GPS Observational Network; GNSS, Global Navigation Satellite System; GPS, Global Positioning System; PBO, Plate Boundary Observatory; TLALOCnet, Trans-boundary, Land and Atmosphere Long-term Observational and Collaborative Network; USGS, U.S. Geological Survey.
*Individual networks may include stations without fully GNSS-compatible equipment and/or may not include all GNSS signals in routine processing.
†UNAVCO data archive, see Data and Resources. See Data and Resources for more information regarding how to access data archived at UNAVCO.
‡VHP, Volcano Hazards Program.
§Northern California Earthquake Data Center (NCEDC, see Data and Resources).
‖SOPAC, Scripps Orbit and Permanent Array Center; CVSRN, Central Valley Spatial Reference Network (Caltrans District 6).
(Continued next page.)

TABLE 1 (continued)
Description of Regional GNSS* Networks Discussed in this Article (See Data and Resources for Network and Archive Websites URLs)

Name	Acronym	Geographic Region	Year Established	Current Number of Stations	Number of Stations within 1.5 km of Seismic Station	Primary Institution for Operations and Maintenance	Data Archive	Notes
Network of the Americas	NOTA	Continental western U.S., Alaska and the Caribbean	2003	1259	58 (see note)	UNAVCO Inc.	UNAVCO	This is a federation of the PBO, COCONet and TLALOCnet networks. 23 sites have UCSD geodetic modules and 35 have borehole seismometers within 1.5 km.
Pacific Northwest Geodetic Array	PANGA	Pacific Northwest	1991	182	15	Central Washington University	PANGA	
Pacific GPS Facility	PGF	Hawaiian Islands	1996	31	9	University of Hawai'i at Mānoa; USGS VHP	UNAVCO, PGF	Two sites collocated with National Weather Service radiosonde network
Puerto Rico Seismic Network	PRSN	Puerto Rico	1997	16	12	Universidad de Puerto Rico – Mayagüez	UNAVCO	
Southern California GNSS Network	SCGN	Southern California	1994	141	59	USGS EHP	UNAVCO	
Scripps Orbit and Permanent Array Center	SOPAC	Southern California and California Central Valley	1992	42	6	SOPAC, CVSRN[‖]	SOPAC	SOPAC also archives RINEX data for about 3000 regional and global network stations

COCONet, Continuously Operating Caribbean GPS Observational Network; GNSS, Global Navigation Satellite System; GPS, Global Positioning System; PBO, Plate Boundary Observatory; TLALOCnet, Trans-boundary, Land and Atmosphere Long-term Observational and Collaborative Network; USGS, U.S. Geological Survey.

*Individual networks may include stations without fully GNSS-compatible equipment and/or may not include all GNSS signals in routine processing.

[†]UNAVCO data archive, see Data and Resources. See Data and Resources for more information regarding how to access data archived at UNAVCO.

[‡]VHP, Volcano Hazards Program.

[§]Northern California Earthquake Data Center (NCEDC, see Data and Resources).

[‖]SOPAC, Scripps Orbit and Permanent Array Center; CVSRN, Central Valley Spatial Reference Network (Caltrans District 6).

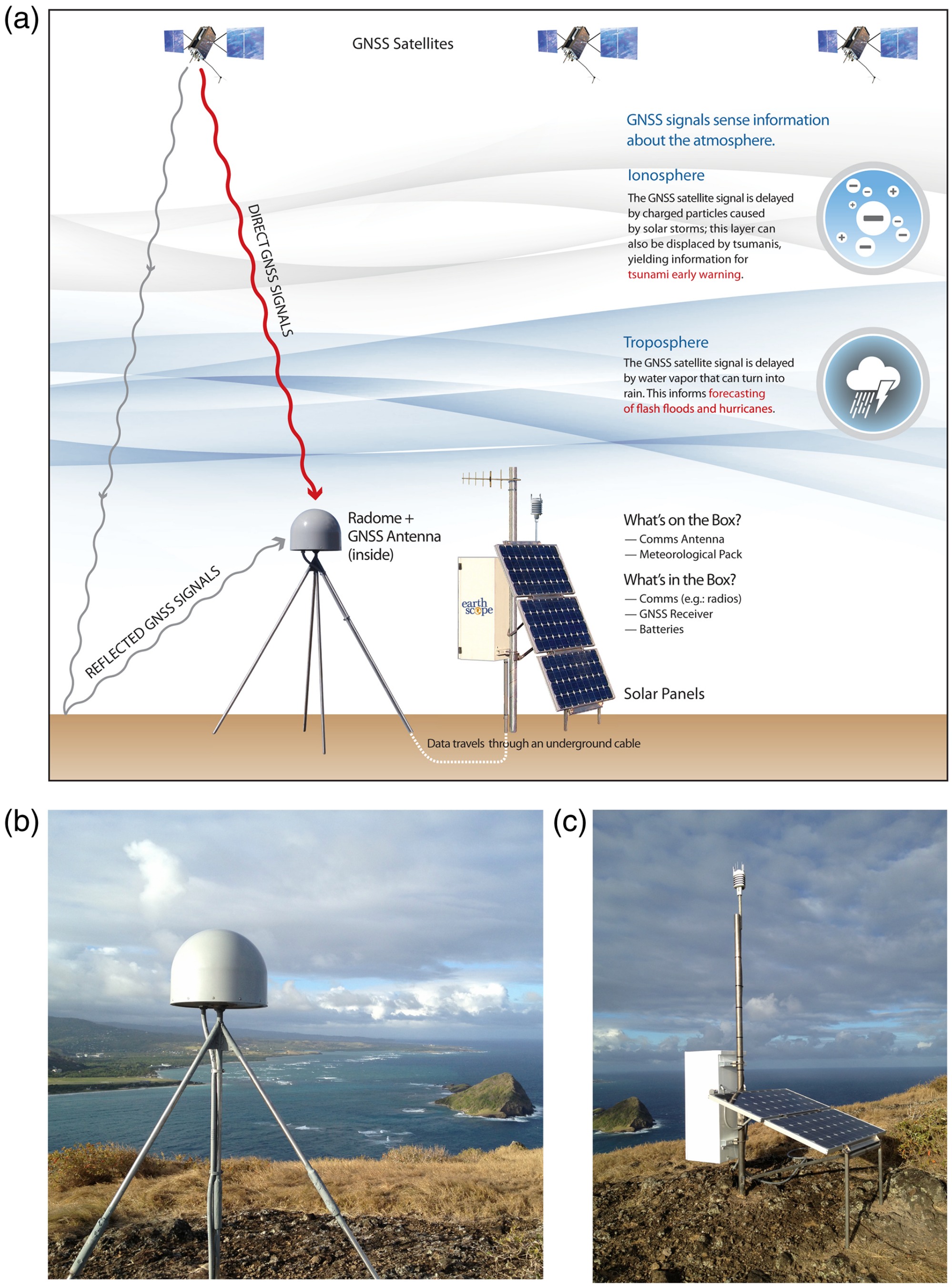

Figure 1. (a) Diagram of typical Network of the Americas (NOTA) permanent Global Navigation Satellite System (GNSS) site configuration. (b) Drilled and braced antenna monument with GNSS antenna. (c) Additional components of this installation include an enclosure for GNSS receiver and communications and power devices, solar panels, and a meteorological instrumentation package. Image credit: UNAVCO Inc. The color version of this figure is available only in the electronic edition.

Because the GNSS signal's travel time is measured at the antenna, the antenna must be mounted stably with respect to the underlying crust. Within and among networks, various types of GNSS antenna monuments are used depending on site characteristics (e.g., geology, weather conditions, available space, and permitting), cost, feasibility of installation methods, and the station's intended purpose. Examples include concrete pillars, pins fixed to rooftops, steel beams driven into sediment, and steel masts or pins cemented into bedrock. The southern California Permanent GPS Geodetic Array (Bock *et al.*, 1997), which evolved into the SCIGN, introduced the use of drilled and braced monuments, a design later adopted by UNAVCO for the PBO (Fig. 1). Although more costly, this design offers improved stability (Mattioli *et al.*, 2007; Mattioli and Jansma, 2007; Langbein, 2008; Hill *et al.*, 2009; Blume *et al.*, 2017; Langbein and Svarc, 2019).

Data transmission methods include cellular modem, radio and microwave, satellite, wireless telemetry, and direct connection to the internet from a host institution. Choice of method depends on desired data volume and transmission rate, allowable latency, available infrastructure, cost, and site-specific conditions (e.g., line-of-sight to repeater sites, radio frequency interference). Typical sampling rates include one sample per 30 or 15 s, 1, 5, and 10 Hz. Receivers can be configured to simultaneously record and transmit data at multiple rates. Raw data may be stored on-receiver in ring buffers and downloaded periodically (e.g., hourly or daily); observations may also be streamed to data centers in real time. Available telemetry bandwidth, along with anticipated applications for the data, are factors that determine sampling rate and data transmission schedule.

Traditionally, data centers carried out centralized processing of downloaded data to estimate a single, three-component position for each station day and analyzed the accumulated position time series to estimate station velocities and other derived products (Bock *et al.*, 2016; Herring *et al.*, 2016; Murray and Svarc, 2017; Blewitt *et al.*, 2018). As high-bandwidth telemetry has

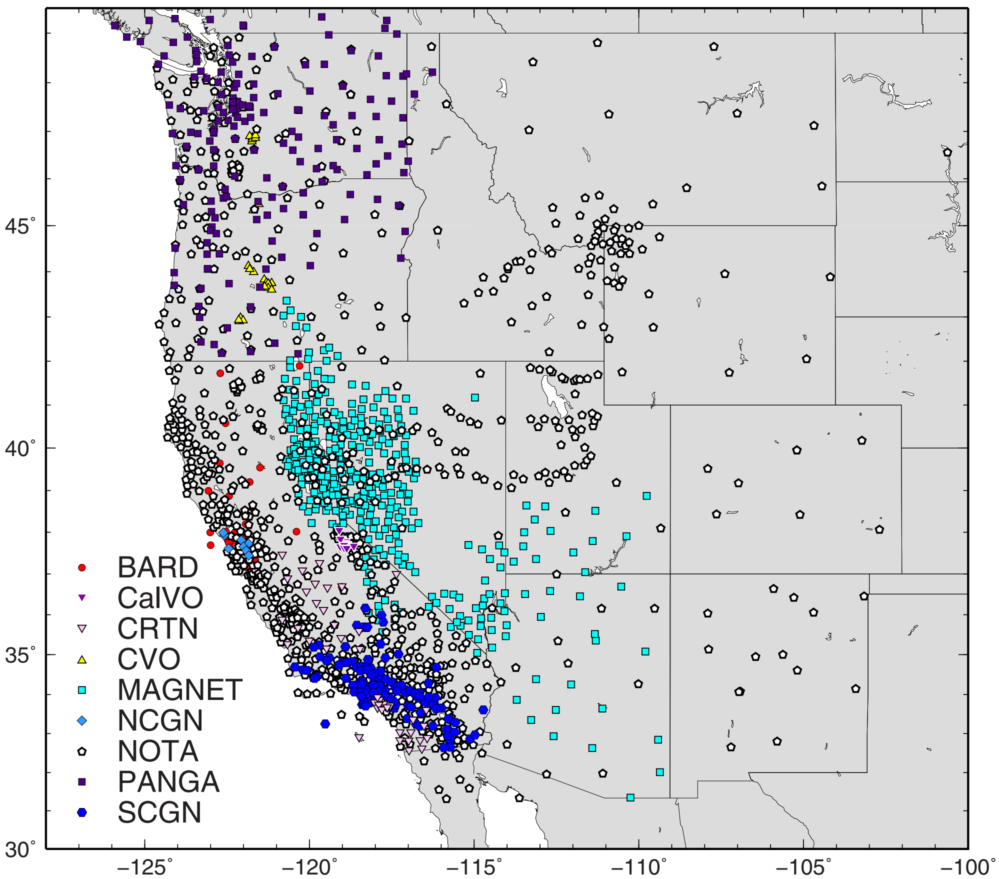

Figure 2. GNSS networks listed in Table 1, the western continental United States (as of May 2019). Network acronyms defined in Table 1. Additional permanent GNSS stations belonging to networks not discussed in this article (e.g., NASA's Global Geodetic Network or the Coast Guard) may be used for research and monitoring but are not depicted on this and the following maps. In areas of dense station coverage, some markers may overlap. The color version of this figure is available only in the electronic edition.

grown more available and affordable, real-time streaming of raw 1 Hz observables has become widespread, providing data for natural hazards monitoring and response, kinematic positioning of a wide variety of platforms, and land surveying. Download of higher sample-rate data (e.g., 5 Hz) is typically done in triggered mode, for example, in the event of an earthquake. In recent years, some receiver manufacturers implemented on-receiver precise positioning and real-time streaming of positions (usually at 1 Hz) using satellite clock corrections delivered directly to the receiver, allowing for stand-alone functionality with potential applications for real-time response to natural disasters. Several regional networks are in the process of upgrading their stations to enable real-time data streaming, use of multiple GNSS constellations, and, in some cases, onboard positioning.

Regional GNSS Networks

U.S. regional GNSS networks cover seismically and volcanically active areas including the San Andreas fault system; Basin and Range province; New Madrid seismic zone; Aleutian, Cascade, and North American–Caribbean subduction zones and associated volcanoes; the Island of Hawai‘i; and Yellowstone (Figs. 2–8, Table 1). The station distributions reflect these networks' initial purpose to monitor ongoing deformation at local to regional scales and to observe distributed crustal strain, fault creep and locking, magma transport, earthquakes, and volcanic eruptions.

Initially U.S. cGNSS networks each covered relatively limited geographic areas, for example, southern California or the Pacific Northwest. In 2003, UNAVCO Inc. began construction of the PBO as part of the National Science Foundation (NSF)-funded EarthScope initiative (Williams *et al.*, 2010), which was designed to observe the 3D, spatiotemporal patterns of crustal strain across the North American-Pacific plate boundary. The project resulted in 875 new cGPS stations throughout the continental U.S. and Alaska in locations chosen to complement existing cGPS networks. In a parallel effort, ~225 existing stations were upgraded and folded into PBO, resulting in the largest U.S. cGPS network designed for scientific purposes. Although a subset of 100 PBO sites provided real-time high-rate data, the standard protocol was 15 s sampling with data downloaded daily.

Around the same time, the University of Nevada, Reno, demonstrated the utility of a scGPS data collection approach. In this mode, monitoring sites are installed by fixing monument pins to bedrock outcrops, which allows GPS instrumentation to be rotated among locations with antenna position repeatability within 1 mm. Instruments can be left onsite for days to years and then moved to another location to enhance spatial coverage. This observation mode offers the flexibility and affordability of temporary deployments with individual daily solution accuracies equivalent to those at continuous stations and velocity precision that is nearly comparable (Blewitt *et al.*, 2009). It works well where resources for construction of cGNSS stations are limited, large geographic areas need to be covered, site accessibility is seasonally limited, and/or low-latency data are not required. The Mobile Array of GPS for Nevada Transtension (MAGNET)

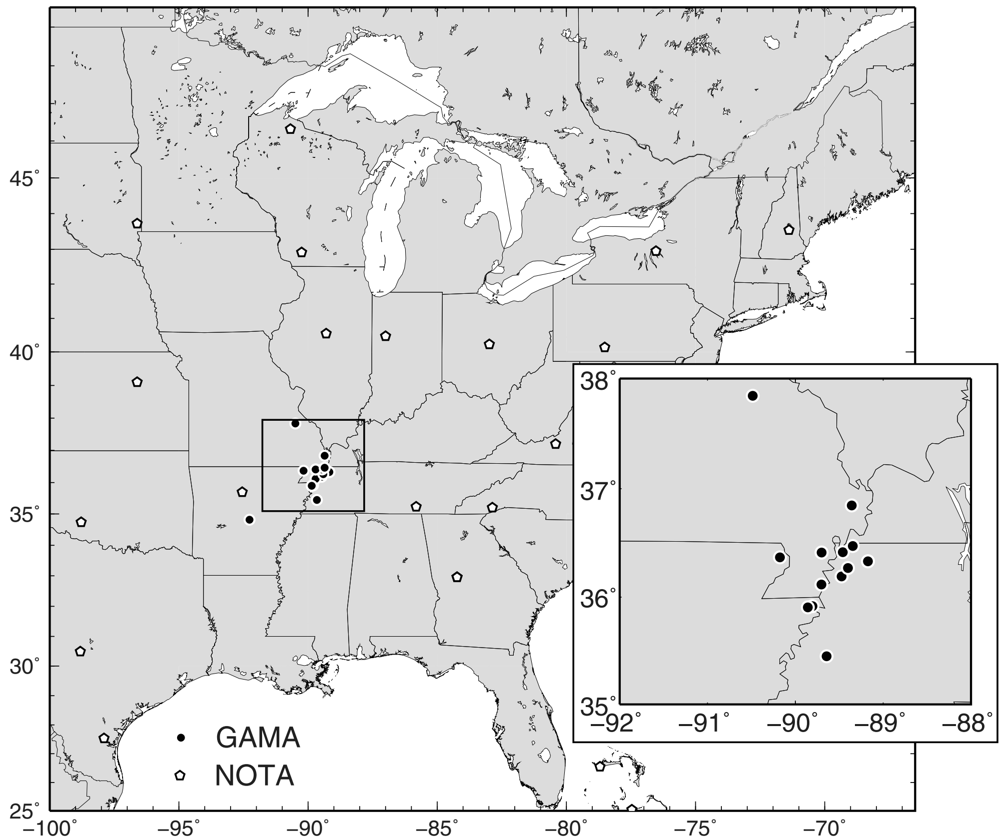

Figure 3. As in Figure 2, central and eastern continental United States. Inset shows stations in the New Madrid Seismic Zone. Location of inset map marked by black box.

network was established in 2004 and now consists of 414 stations that touch five western U.S. states (Nevada, California, Utah, Arizona, and Oregon).

GNSS network funding sources have included: NSF, U.S. Geological Survey (USGS), National Aeronautics and Space Administration (NASA), other federal, state and local agencies, partner universities, and matching funds provided by institutions such as universities that have the primary responsibility for operation and maintenance of some networks. The Pacific Northwest Geodetic Array (PANGA) is an example of a multiagency cooperative network designed to provide data for both crustal deformation research and professional land surveyors (PLSs). The costs of most stations comprise not only the electronic hardware but also permitting, installation, power, telemetry, and routine maintenance. Thus, a data-sharing synergy naturally arose between the surveying and research communities in the Pacific Northwest, subject to the criteria that data be telemetered in real time (for PLS applications) and that station monuments be very stable (for tectonics research). The engagement of the PLS community has enabled expansion and densification of the PANGA footprint and upgrading of all stations to real-time data transmission. The California Real Time Network (CRTN), with more than 1300 registered users, distributes real-time data from several networks for a broad range of applications, including surveying, precision agriculture, airborne light detection and ranging, and other activities requiring real-time dynamic positioning, as well as for scientific research and natural disaster early warning.

Recognizing that deformation sources like the Cascadia subduction zone traverse international borders, PANGA incorporated stations in both the U.S. and Canada, becoming an early example of international collaboration in regional cGNSS network development. UNAVCO has long supported geodetic network implementation and data collection efforts throughout the globe. In October 2018, PBO became federated with the Trans-boundary, Land and Atmosphere Long-term Observational and Collaborative Network (TLALOCNet, Cabral-Cano *et al.*, 2018) in Mexico and the Continuously Operating Caribbean GPS Observational Network (COCONet, Braun *et al.*, 2012) to form a unified Network of the Americas (NOTA). The majority of NOTA sites provide real-time data, with many already enhanced to be fully GNSS capable.

Regional GNSS Networks' Impact on Crustal Deformation Research and Monitoring

Data from the regional GNSS networks in Table 1 underlie a wide range of research and have led to unexpected discoveries in the fields of crustal deformation and beyond. These accomplishments would not have been possible without the commitment of network operators to freely sharing data, both raw and processed, with the scientific community. Although this practice existed to varying degrees early on, the PBO adopted a systematic protocol for providing raw data and derived products without delay and free of charge. This philosophy served as a model for other network operators. UNAVCO also promoted the use of digital object identifiers as part of its open data policy (Pritchard *et al.*, 2012). Beyond contributing raw data to online archives (Table 1), most networks offer position time series at various sample rates and derived products such as station velocities, seasonal motion, coseismic offsets, and postseismic decay (e.g., Bock *et al.*, 2016; Herring *et al.*, 2016; Murray and

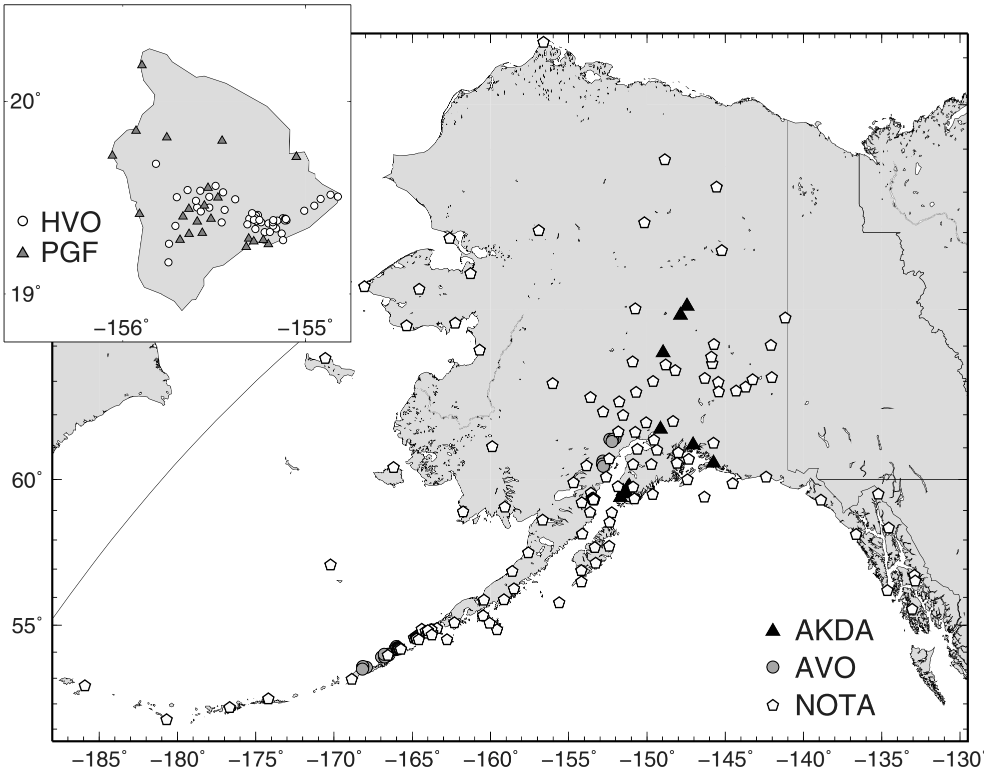

Figure 4. As in Figure 2, Alaska and Big Island of Hawai'i. Inset shows the GNSS networks on the Big Island of Hawai'i.

Beginning with the 1992 M_w 7.2 Landers earthquake (Blewitt *et al.*, 1993; Bock *et al.*, 1993), the regional cGNSS networks recorded coseismic displacements associated with several significant earthquakes in the western U.S. and Alaska. As demonstrated by Langbein *et al.* (2006) for the 2004 M_w 6 Parkfield earthquake, continuously recorded data, especially with subdaily or 1 Hz positioning, enable separating coseismic from immediate postseismic signals, which otherwise would be aliased. In its routine GNSS data analysis, UNAVCO's Geodesy Advancing Geosciences facility recognizes 41 earthquakes since 1999 that potentially cause offsets in GNSS time series and provides estimated displacements (Herring *et al.*, 2016).

The installation of regional cGNSS networks worldwide was central to discovering a variety of slow-slip behavior ranging from days to years in duration. Indeed, although it would not be recognized for another decade, the first station of the PANGA array was installed by the Natural Resources Canada Pacific Geoscience Center along the southern coast of Vancouver Island during a 1992 slow-slip event (SSE; Dragert and Hyndman, 1995; Miller *et al.*, 2002). Eventually, daily position time series from cGPS sites in southern British Columbia and northern Washington permitted the discovery of repeated SSEs in the northern portion of the Cascadia subduction zone (Dragert *et al.*, 2001), and the signature of SSEs was found in data from cGPS sites along the entire Cascadia margin (Szeliga *et al.*, 2008). Where cGNSS and seismic networks overlap, some SSEs have been found to be accompanied by tectonic tremor in combined episodic tremor and slip events (e.g., Rogers and Dragert, 2003; Schwartz and Rokosky, 2007; Peng and Gomberg, 2010; Bürgmann, 2018). The availability of daily cGPS position estimates with millimeter-level accuracy enabled detailed studies of the spatial distribution and temporal evolution of episodic SSEs across the Cascadia subduction zone (e.g., Bartlow *et al.*, 2011), which is important for clarifying the role of SSEs in earthquake hazard assessment.

Similarly, the availability of cGPS data allowed for the discovery of SSEs on the south flank of Kīlauea that were previously unknown from campaign GPS observations (Cervelli *et al.*, 2002). Kīlauea's SSEs occur on a subhorizontal decollement

Svarc, 2017; Blewitt *et al.*, 2018). Increasingly sophisticated data access interfaces enabled easier data discovery and visualization, in turn empowering a broader range of scientists and educators to use these observations in innovative ways (Zietlow *et al.*, 2016; Blewitt *et al.*, 2018). Here, we highlight some contributions of U.S. regional GNSS networks to crustal deformation research with a focus on seismotectonic and volcanic processes; Bock and Melgar (2016) provide a global overview of GNSS-based research.

As the footprint of GNSS networks has grown, and particularly with the establishment of the PBO, it has become possible to develop broadscale kinematic and dynamic models of the spatial and temporal patterns of deformation (e.g., Flesch *et al.*, 2007; Kreemer and Hammond, 2007; Pollitz *et al.*, 2008; Bird, 2009; Parsons and Thatcher, 2011; Kreemer *et al.*, 2012; Petersen *et al.*, 2014). The frequent (i.e., daily) sampling of position time series enabled better characterization of temporally correlated noise processes (Langbein, 2008; Davis *et al.*, 2012), in turn resulting in more realistic characterization of velocity uncertainties. The resulting horizontal and vertical velocity fields provided a new source of data to constrain deformation models for hazard assessment. For example, the Uniform California Earthquake Rupture Forecast, v.3 was the first to incorporate geodetically constrained fault-slip rates and strain rates that leveraged the expanded spatial coverage of GNSS sites in California (Parsons *et al.*, 2013).

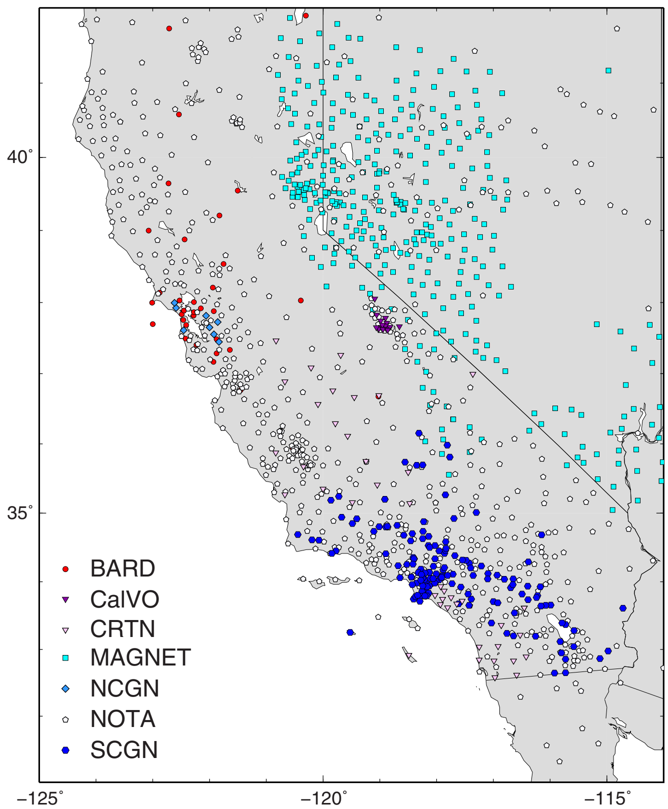

Figure 5. As in Figure 2, close-up of California and Nevada. The color version of this figure is available only in the electronic edition.

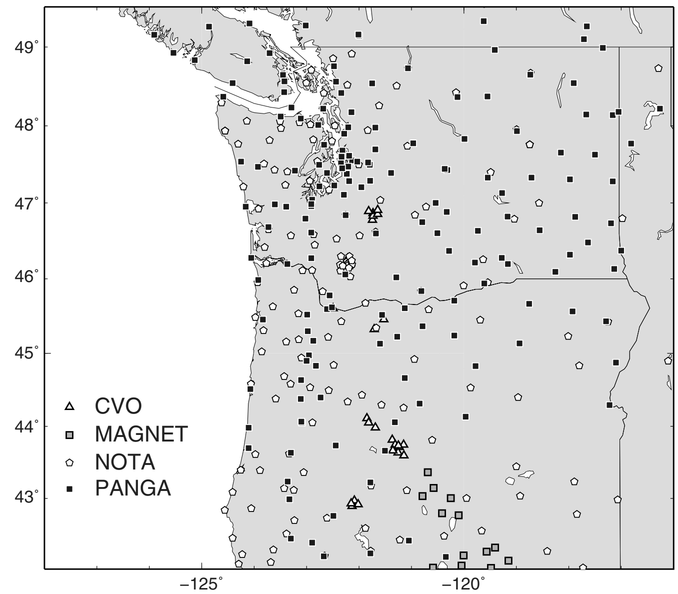

Figure 6. As in Figure 2, close-up of Oregon and Washington.

~8 km beneath the southern flank of the volcano, last about two days, and produce slip events equivalent to an M_w 5.4–6.0 earthquake (Brooks *et al.*, 2006). Unlike many subduction zone SSEs, however, Kīlauea's SSEs occur without detectable seismic signals (Montgomery-Brown *et al.*, 2009). Thus, cGNSS observations are the primary means of observing these SSEs. cGPS data also revealed repeated, propagating SSEs in the Alaska–Aleutian subduction zone downdip of the coseismic rupture area of the 1964 M_w 9.2 earthquake. With durations of 2–9 yr, these events may release most of the interseismically accumulated slip deficit on a portion of the megathrust (Ohta *et al.*, 2006; Fu, Liu, and Freymueller, 2015; Li *et al.*, 2016).

cGNSS data, especially in combination with other data types including Interferometric Synthetic Aperture Radar, gravity, tilt, and leveling, have become an indispensable tool for volcano monitoring (Poland *et al.*, 2017). For example, GPS observations enabled tracking the spatiotemporal evolution of unrest during the 2004 eruption of Mount St. Helens (Lisowski *et al.*, 2008), and illuminated ongoing deformation at a time of seismic quiescence during the 2006 eruption of Augustine volcano (Cervelli *et al.*, 2006). cGPS data recorded multiple periods of uplift at Long Valley caldera, interpreted as arising from magma intrusion at depth (Battaglia *et al.*, 1999; Montgomery-Brown *et al.*, 2015), as well as capturing multiple deformation events at Yellowstone attributed to magmatic intrusions (Chang *et al.*, 2010; Farrell *et al.*, 2010).

Although beyond the scope of this article, data from the cGNSS networks discussed here also revealed deformation signals arising from a variety of hydrologic loading processes (Bawden *et al.*, 2001; King *et al.*, 2007; Amos *et al.*, 2014; Argus *et al.*, 2014; Borsa *et al.*, 2014; Fu, Argus, and Landerer, 2015; Argus *et al.*, 2017), some of which may influence seismicity patterns through the crustal stresses they impart (e.g., Johnson *et al.*, 2017; Kraner *et al.*, 2018; Kreemer and Zaliapin, 2018). cGNSS stations can augment tide-gauge networks for tracking global sea-level change by providing measures of vertical land motion that can be used to obtain absolute sea-level measurements in a terrestrial reference frame (Foster, 2015) and through analysis of cGNSS signal-to-noise ratio to directly estimate local sea level (Larson *et al.*, 2013). cGNSS data also provided a unique set of observations for estimating snow depth, soil moisture, permafrost, and other near-surface characteristics that affect GNSS signal reflection (Larson, 2016).

Real-Time GNSS

An early demonstration of the value of rapidly estimated earthquake ground displacement from GPS followed the 1992 M_w 7.2 Landers (Shen *et al.*, 1994) and 1994 M_w 6.7 Northridge (Hudnut *et al.*, 1996) earthquakes. In the Northridge case, although only a few cGPS stations were operating in the vicinity of the epicenter, their observations, combined with postearthquake campaign GPS data from nearby benchmarks, provided coseismic displacements that were used to infer a finite-fault slip model within eight days of the event (K. Hudnut and M. Murray, personal comm., IGSMail-466, 1994, see Data and Resources). Initial seismological observations and diffuse

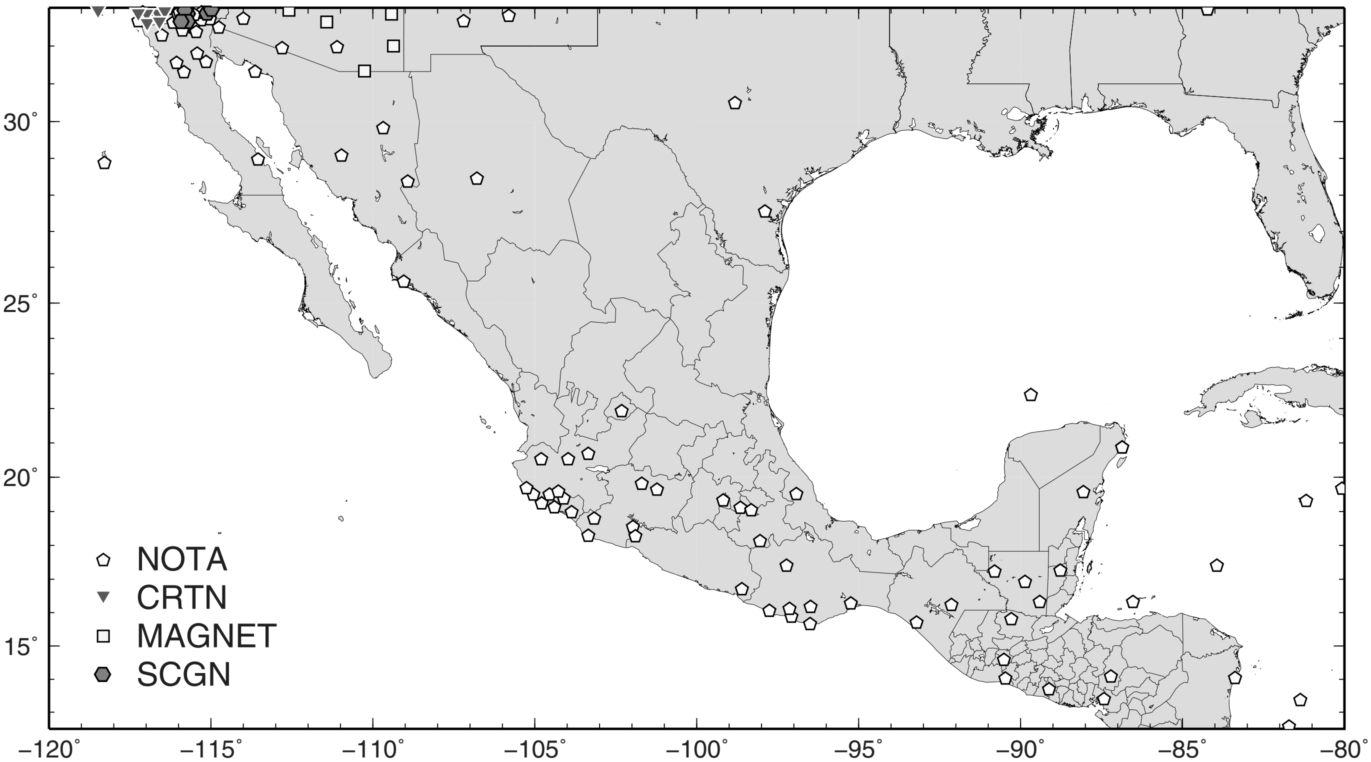

Figure 7. As in Figure 2, Mexico.

aftershock locations poorly resolved the orientation of the blind-thrust fault, but the geodetic displacements clearly favored a south-southwest-dipping fault, suggesting the advantages of combined seismological and geodetic observations for rapid earthquake source characterization. Today similar results can be obtained in minutes to seconds from real-time data.

Observations recorded during the Hector Mine (Nikolaidis *et al.*, 2001), Denali (Larson *et al.*, 2003; Bock *et al.*, 2004), and Parkfield (Langbein and Bock, 2004) earthquakes further demonstrated the potential value and capabilities of high-rate (e.g., 1-Hz-or-higher sampling rates) and real-time positioning for earthquake response. Rhie *et al.* (2009) envisioned the use of real-time GNSS data to rapidly characterize earthquake sources to provide information on source finiteness and rupture directivity that would improve ShakeMap estimates of peak ground velocity (PGV). Despite using simplistic rupture model assumptions to enable rapid computation, the method was able to match Northridge earthquake PGV observations sufficiently well to demonstrate the potential contribution of GNSS-derived models for use in emergency response.

In 2006, development began on the U.S. EEW system, ShakeAlert (Given *et al.*, 2018), employing algorithms to rapidly characterize the earthquake source using the first few seconds of the P wave. However, as observed during the 2011 M_w 9.0 Tohoku-Oki earthquake and other large events globally, real-time earthquake magnitude estimates derived from seismic data alone are known to saturate above $\sim M_w$ 7 (Hoshiba and Ozaki, 2014). GNSS displacements enable nonsaturating magnitude estimates for large events and provide information on source finiteness, both of which have the potential to improve the accuracy of ground-motion calculations for EEW purposes (e.g., Crowell *et al.*, 2013; Grapenthin *et al.*, 2014; Minson *et al.*, 2014; Ruhl *et al.*, 2017). Blewitt *et al.* (2006) demonstrated that near-real-time GPS positions from data collected at a 30 s sampling interval would have enabled more accurate and timely warnings of the impending tsunami resulting from the 2004 M_w 9.1 Sumatra earthquake. Allen and Ziv (2011), using real-time GPS from the 2010 M_w 7.2 El Mayor–Cucapah earthquake, showed that long-period information lost in accelerometer data was retained in the 1 Hz geodetic time series at a site with collocated GPS and seismic instrumentation. The findings of Grapenthin *et al.* (2017) and Ruhl *et al.* (2017) suggest that cGNSS networks could be a valuable augmentation to EEW systems in regions with sparse seismic network coverage. Some studies conclude it is possible to obtain nonsaturating magnitude estimates for large earthquakes using high-rate GNSS data while rupture is ongoing (e.g., Melgar *et al.*, 2015; Melgar and Hayes, 2017; Goldberg *et al.*, 2018). The existence of rupture determinism remains a topic of active debate with important implications for EEW. Ongoing ShakeAlert development includes assessing the contribution that GNSS data can make to EEW, optimizing processing strategies to reduce latency and increase robustness, and further developing algorithms that utilize these observations to improve real-time ground-motion prediction (Murray *et al.*, 2018).

Motivated by the aforementioned research findings and operational demands, cGNSS networks are transitioning to real-time 1 Hz data collection and streaming. The 2009

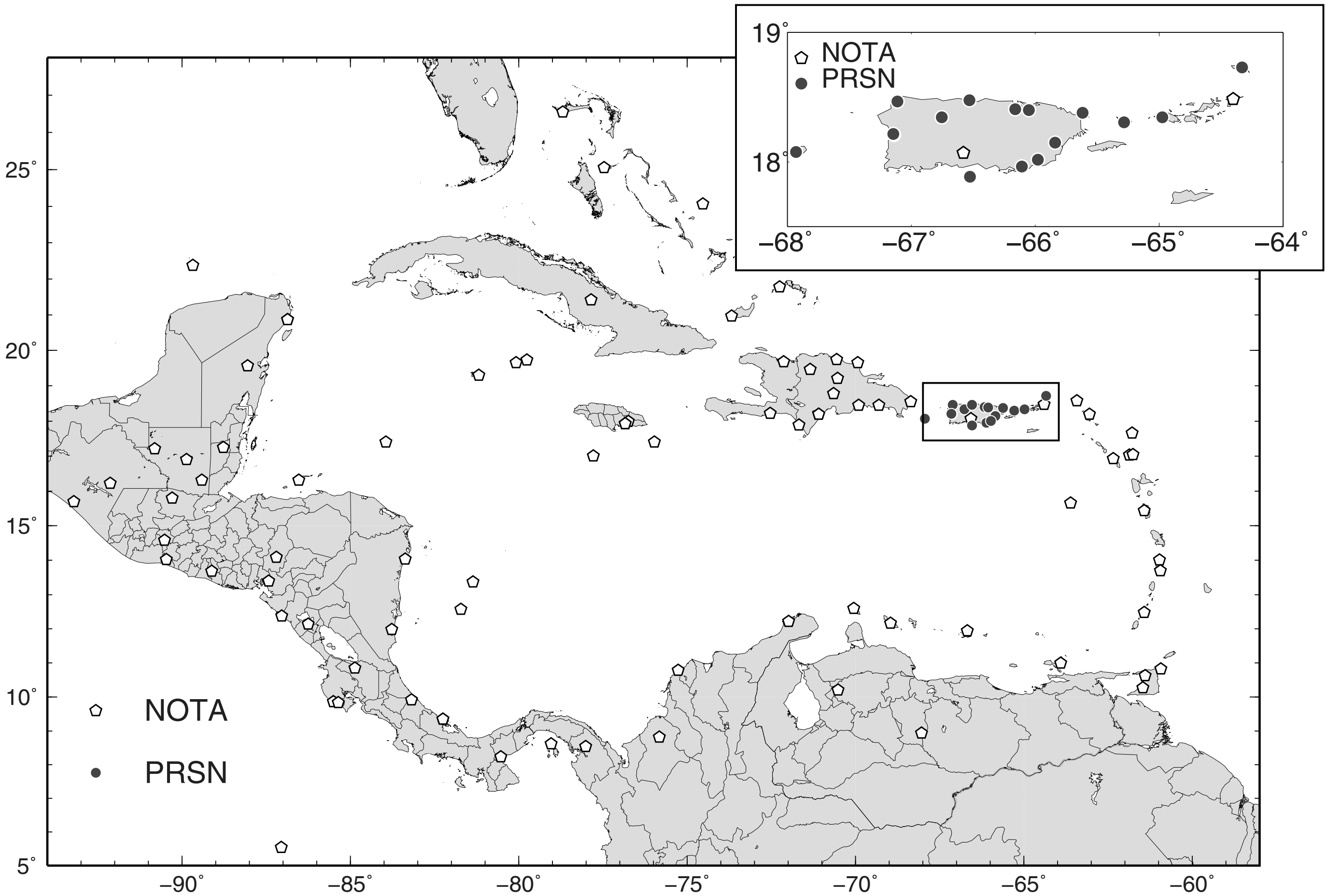

Figure 8. As in Figure 2, the Caribbean region. Inset shows stations in Puerto Rico. Location of inset map marked by black box.

American Recovery and Reinvestment Act (ARRA) provided a significant source of funding for this effort, supporting the establishment of the USGS Northern California GNSS Network, conversion of 230 PBO sites to real time under the Cascadia Initiative, and upgrade of PBO stations for monitoring at Yellowstone caldera (in collaboration with USGS). ARRA-funded projects also expanded the number and improved the robustness of real-time GNSS stations in the USGS Southern California GNSS Network (SCGN), Bay Area Regional Deformation (BARD), CRTN, and PANGA networks. In parallel, the National Ocean and Atmospheric Administration (NOAA) funded the real-time upgrade of some PBO sites for weather forecasting. Through an Urban Area Security Initiative grant, 41 real-time stations were added to the SCGN in 2016. As it became evident that real-time streaming was an efficient method of data retrieval and network operations, NSF funded additional PBO upgrades between 2008 and 2018. As of 2019, over 800 stations in NOTA provide real-time high-rate data. Further improvements to real-time GNSS infrastructure in USGS and partner networks (PANGA, BARD, and NOTA) are in progress as part of the ShakeAlert project.

Table 2 summarizes real-time data generated by the regional GNSS networks discussed in this article. Several networks provide the raw data streams through Ntrip casters (Weber *et al.*, 2005), and data centers often process real-time data from multiple networks, for example, to provide redundant data sources for real-time monitoring and response. Some networks also provide web portals for viewing real-time processed positions via dynamically updated plots (Fig. 9). UNAVCO presents data and interpretation on its website's geophysical event response pages (see Data and Resources), including displacement waveforms from real-time processing, earthquake source information estimated from these data, and updated models incorporating observations from nonreal-time stations (Fig. 10).

GNSS data are increasingly important for volcano monitoring (e.g., Cervelli *et al.*, 2006, 2010; Fournier *et al.*, 2009). The variety of processes that can be active during an eruptive crisis, and the speed at which a sequence of events can unfold, make it challenging yet critically important to quickly develop interpretive models for public safety partners. During the 2018 eruption and earthquake sequence at Kīlauea volcano, real-time GPS data were central to monitoring and generating short-term hazard forecasts (Neal *et al.*, 2019). This period of unrest involved both a flank eruption in Kīlauea's lower east rift zone and collapse of the summit caldera ~40 km to the west. The Hawaiian Volcano

TABLE 2
Real-Time GNSS Availability

Name	Acronym	Number of Stations Providing Real-Time GNSS Data*	Subset of Real-Time Stations that Provide Multiconstellation GNSS Data	Data Formats	Real-Time Raw Data Access	Notes
Bay Area Regional Deformation network	BARD	33	5	BINEX, RTCM3	see Data and Resources	Remaining sites to be upgraded to GPS +GLONASS by August 2020
California Volcano Observatory Long Valley Network	CalVO	16	16	RTCM3	Internal use	
California Real Time Network	CRTN	42 (see note)	42	RTCM3	IP = 132.239.154.80:2103 (southern California), IP = 132.239.152.175:2103 (northern California)	RTCM3 data rebroadcast from multiple NTRIP servers, for a total of 600 stations, ~200 of which provide multi-GNSS data
Cascades Volcano Observatory	CVO	28	Variable	BINEX or RTCM3	Internal use	
GPS Array for Mid-America	GAMA	9	3	RTCM3	Real-time streams for stations HCES, MCTY, STLE, CVMS, NWCC, PTGV, NMKM, and RLAP available from Tennessee Department of Transportation broadcast server IP: 170.143.44.6, requires authentication	
Hawaiian Volcano Observatory	HVO	42	0	BINEX	Internal use	Sampling rate for real-time data is 1 Hz or 5 samples per second, depending on station
Northern California GNSS Network	NCGN	8	0	BINEX	see Data and Resources	
Network of the Americas	NOTA	891	370	PPP, BINEX, RTCM3	see Data and Resources	
Pacific Northwest Geodetic Array	PANGA	163	149	RTCM3	see Data and Resources	
Pacific GPS Facility	PGF	4	1	RTCM3	Internal use	Public access to real-time streams from 10 sites planned by January 2020
Puerto Rico Seismic Network	PRSN	16	3	BINEX, RTCM2, RTCM3	see Data and Resources	
Southern California GNSS Network	SCGN	120	44	BINEX	see Data and Resources	

GLONASS, Global Navigation Satellite System.
*Sampling rate is 1 Hz for all networks unless otherwise indicated.

Observatory (HVO) supplemented its backbone GPS monitoring network with semicontinuous stations, and these stations were rapidly integrated into the processing framework. The real-time GPS data, along with migrating seismicity, were among the first indications of subsurface dike propagation down the rift zone. The GPS data were used to monitor the growth of

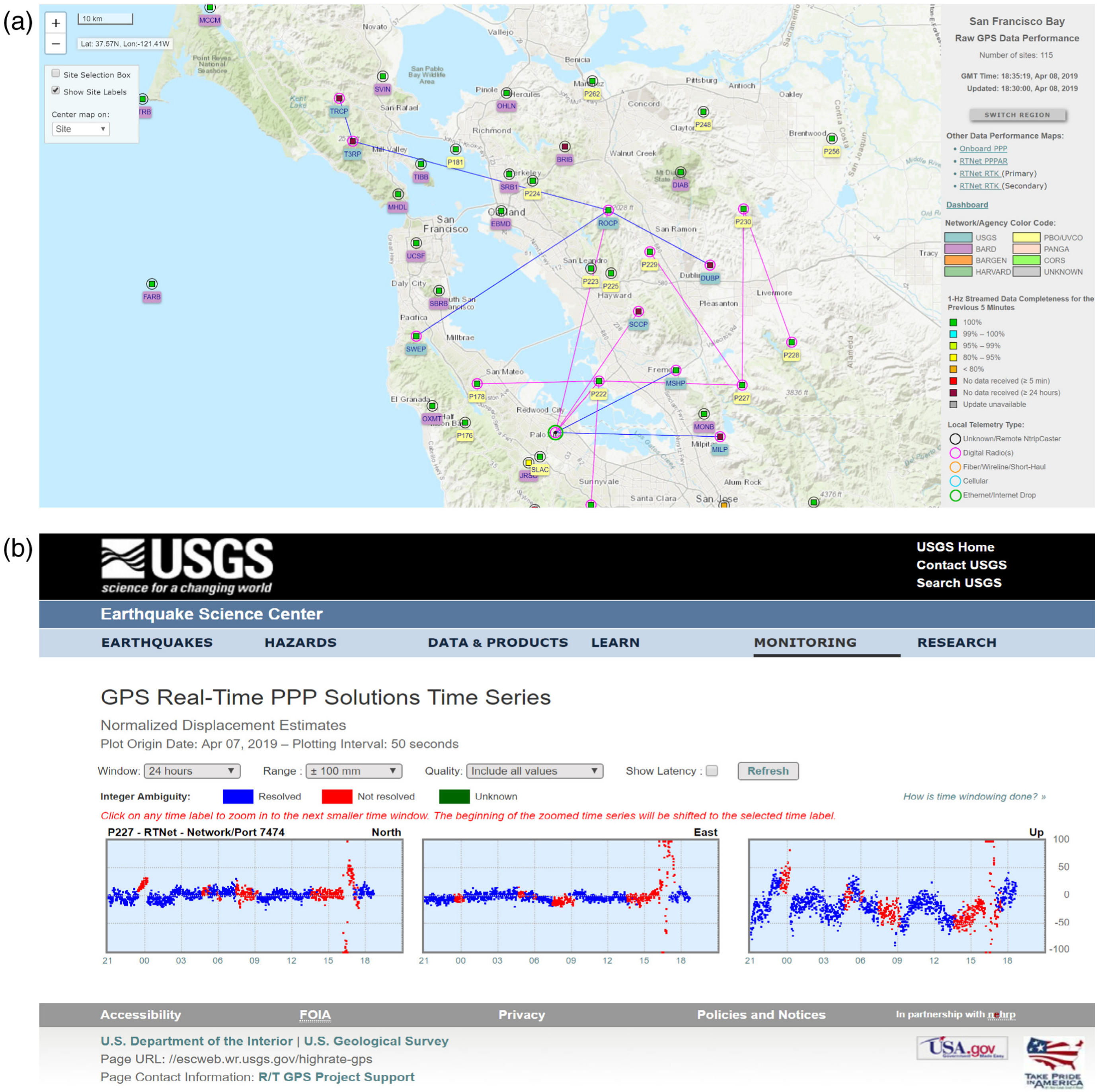

the intrusion and infer continued dike opening over a few days following the initial fracture. At the summit, the GPS data provided unique information on the almost daily collapse events that included up to 8 m of subsidence and repeated displacements of stations just beyond the collapsing blocks within the caldera. This was the first use of real-time GPS data by HVO for eruption response and provided proof of concept for the utility of this information during a volcanic crisis.

The natural hazard applications of real-time GNSS data reach beyond EEW and volcano monitoring. For example, Melgar and Bock (2015) demonstrated that tsunami propagation predicted from kinematic earthquake rupture models

Figure 9. Example web interface for real-time GNSS. This website (see Data and Resources) includes information regarding the GNSS stations for which the USGS Earthquake Hazards Program processes real-time data. (a) Map interface for real-time stations in the San Francisco Bay Area. Clicking station markers provides additional information regarding data completeness and receiver diagnostics. Menu on the right provides access to position time series from real-time processing. (b) Example time series. The color version of this figure is available only in the electronic edition.

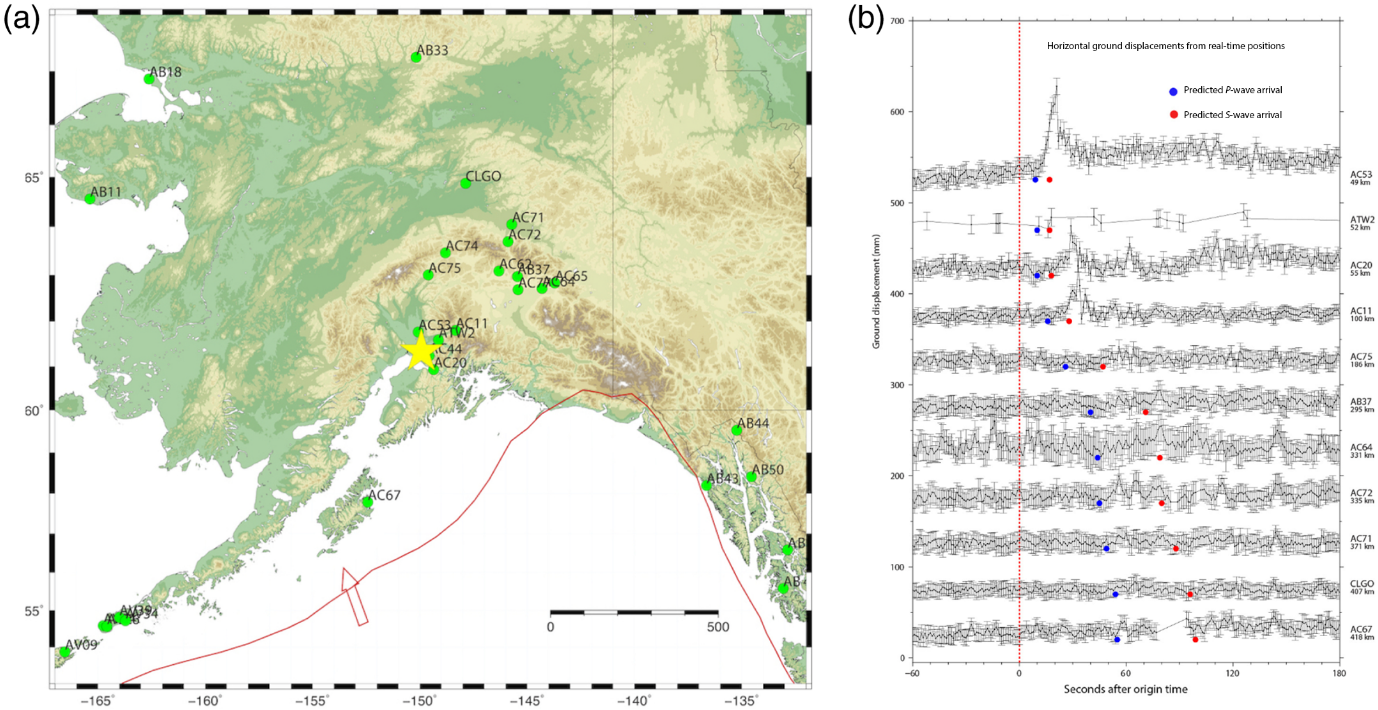

Figure 10. Example of real-time ground displacement time series recorded during the 30 November 2018 M_w 7.1 earthquake, northwest of Anchorage, Alaska. Plots depicting data and interpretation are included in UNAVCO's geophysical event response web pages (https://www.unavco.org/projects/project-support/geophysical-event-response/geophysical-event-response.html, last accessed May 3, 2019). (a) Sites providing real-time data. (b) 1 Hz horizontal displacement time series calculated from real-time GNSS data. Vertical dashed line: earthquake origin time. The color version of this figure is available only in the electronic edition.

constrained by real-time GPS, strong-motion, seafloor pressure, and GPS buoy data could provide accurate local runup estimates within minutes of rupture nucleation. Melgar *et al.* (2016) subsequently showed that even with simpler source models, useful local tsunami warning could be possible using data from land-based GNSS and seismic stations. The NASA-funded Real-Time Earthquake Analysis for Disaster Mitigation (READI) project, in collaboration with NOAA, is building a system to be used by NOAA's tsunami warning centers that combines real-time GNSS and seismic data to rapidly locate and characterize earthquakes (Stough and Green, 2016). The earthquake source information provides input to tsunami initiation and propagation models from which evacuation warnings could be generated for coastal communities.

Measuring ionospheric disturbances using GNSS potentially provides another method to track tsunami propagation (Occhipinti *et al.*, 2013; Komjathy *et al.*, 2016). Tsunamis generate atmospheric gravity waves that, in turn, trigger ionospheric disturbances that travel outward from the earthquake source region. The ionosphere is dispersive, causing frequency-dependent travel-time delays in GNSS signals. These delays can be used to estimate the total electron content (TEC), a measure of the electron density between a receiver and satellite. Savastano *et al.* (2017) demonstrated that real-time GNSS tracking of TEC perturbations can provide information on tsunami propagation that is consistent with that generated by NOAA's current real-time forecast system.

Knowledge of TEC perturbations is also important for monitoring space weather, such as solar flares and geomagnetic storms, that can affect power grids, satellite communication, cell phone networks, aviation, and GNSS positioning systems. NOAA's Space Weather Prediction Center uses UNAVCO's real-time GNSS streams to generate maps of TEC, which are analyzed for anomalies to issue alerts and storm watches.

Real-time GNSS data can also contribute to weather forecasting. Water vapor in the atmosphere delays the GNSS signals (Bevis *et al.*, 1994; Radhakrishna *et al.*, 2015), and this delay can be used to infer the precipitable water vapor (PWV). Knowledge of PWV is critical for accurate, operational weather forecasting, and data from GPS sites have proven to be valuable during extreme weather events (Smith *et al.*, 2007). California GNSS networks have been used to track summer monsoons (Moore *et al.*, 2015) and atmospheric rivers (Wang *et al.*, 2019), providing input to successful forecasts of flash flooding. The study of atmospheric processes was one motivation in designing TLALOCNet and COCONet (Braun *et al.*, 2012; Cabral-Cano *et al.*, 2018), as well as the University of Hawai'i GNSS network on the Big Island of Hawai'i (e.g., Foster and Bevis, 2003; Foster *et al.*, 2003). Currently UNAVCO's raw data streams are being processed in real time to extract the zenith total delay, a measure of signal delay used to estimate the PWV. PWV estimates are then assimilated into NOAA's numerical weather prediction models. As is true for EEW and tsunami warning systems, such models depend on dense, accurate, and low-latency GNSS observations.

Integration with Seismic Networks

As stated in the ANSS strategic plan (USGS, 2017), further integration of GNSS and seismic networks would support stated ANSS goals by promoting joint use of the two data types to better characterize earthquake sources and ground motion and by providing opportunities to leverage resources for building and maintaining network infrastructure.

Unlike seismic data, GNSS positions directly record both the dynamic displacement and static offsets during an earthquake but at low-temporal resolution with centimeter-level precision. Bock *et al.* (2011) developed a Kalman-filter-based approach to combine strong-motion records and GNSS positions from collocated instruments, producing a so-called seismogeodetic position stream. In this technique, GNSS displacements, with their longer period stability and accuracy, constrain the integration of higher sample rate, lower noise threshold seismic data. The resulting displacement waveforms retain both the *P*-wave arrival and static offsets. Seismogeodetic positions generated in real time would provide input for magnitude scaling relationships or rapid finite-fault modeling, both of which could produce substantially more accurate earthquake source parameter estimates for calculating ground motion in an EEW context (e.g., Crowell *et al.*, 2016) and for tsunami warning (Melgar and Bock, 2015).

Incorporation of algorithms that use GNSS data, alone or jointly with seismic data, is an area of active research and development within ShakeAlert. Some of the geodetic EEW algorithms currently under development exclusively use GNSS position time series to characterize the earthquake source in real time, only using seismic data indirectly to trigger initiation of geodetic modeling. Approaches that make joint use of seismic and geodetic data are also under development, such as the integrated use of the Finite-Fault Rupture Detector (FinDer; Böse *et al.*, 2017) and Bayesian Evidence-based Fault Orientation and Real-time Earthquake Slip (BEFORES; Minson *et al.*, 2014) algorithms or magnitude estimation via scaling laws that use seismogeodetic positions (Crowell *et al.*, 2013).

In addition to the scientific and earthquake response benefits, collocating seismic and GNSS stations can support more efficient network construction, operation, and maintenance through shared power and telemetry systems, dual-use site permits, and consolidated visits to field sites. Fully achieving these efficiencies is most successful with careful planning and coordination among network operators and data users. For example, the physical requirements for seismic and geodetic stations, though similar, are not identical. Minimizing anthropogenic and natural noise sources is a priority for seismic sites, whereas unobstructed sky visibility and low multipath are critical for optimal GNSS data collection. The telemetry bandwidth and power requirements for collecting and transmitting the two data types in real time also differ. Power and communications infrastructure must be designed to meet the needs of both while minimizing system complexity to facilitate maintenance and promote network robustness. Even stations separated by 1–2 km can still be considered collocated for some applications (Bock *et al.*, 2011; Crowell *et al.*, 2013) and could offer some of the installation, operation, and maintenance efficiencies achieved by fully collocated instrumentation.

The spatial footprints of regional GNSS and seismic networks overlap. In some cases, the same institution operates both types of networks, and infrastructure for power supply, radios, and data transmission are shared. Several of the regional GNSS networks discussed here include stations that are collocated with broadband and/or strong-motion seismometers (Table 1). Further integration of seismic and geodetic networks is underway to support anticipated applications for co-located seismic and GNSS observations. In the past two years, USGS has funded the upgrade of ~54 NOTA stations distributed between central California and Seattle to include seismic instrumentation operated by ShakeAlert partner institutions. Upgrades to power and communication systems at these sites will enable direct real-time high-rate GNSS data flow to ShakeAlert data centers, concurrent with seismic data streams. The data will continue to flow to UNAVCO's data operations center through an independent data path, providing system redundancy.

Over the past decade individual network operators developed methods to bring real-time high-rate GNSS data from field stations to their respective data centers and to integrate these data into their existing systems as needed for follow-on applications. The increased focus on joint use of real-time seismic and geodetic data, along with expansion of co-located stations, has prompted the evolution of data management software and formats from network-specific solutions to standardized approaches that support monitoring and event response activities shared by multiple regional networks. For example, real-time GNSS position streams from ShakeAlert partner networks are transmitted with a standardized format and messaging protocol. These data are stored and accessed using the EarthWorm software and associated data storage architecture that was already in use for seismic data (Hernández and Martínez, 2018; López *et al.*, 2018).

Looking Ahead

Recent and ongoing developments in GNSS receiver technology, data analysis methods, and the underlying observational and computational infrastructure enable and inspire a variety of future directions for regional GNSS networks. Here we highlight a few examples.

Instrumentation

Current real-time network operations primarily utilize data-center-based processing systems; raw data from field stations stream to a centralized location where they are processed in real time and the solutions are redistributed. On-receiver GNSS data processing, now offered by some manufacturers, enables a simpler system in which stations can independently stream positions directly to users. For natural disaster response, a hybrid system in which raw data from all sites are processed at the data center while a subset of stations with receivers capable of on-board processing also stream position estimates directly to the institutions that generate alerts would provide redundancy and failover.

New types of networks

Maintaining and expanding the spatial coverage of GNSS networks that provide open access to data through robust acquisition and transmission systems will support basic research as well as monitoring to mitigate the impact of natural hazards. The availability of real-time GNSS data, along with observations from collocated seismic instruments and/or other geophysical sensors, will prompt further algorithm development and creation of new approaches to improve rapid assessment of earthquakes, eruptions, tsunamis, and their impacts (e.g., Blewitt *et al.*, 2018). Construction, operation, and maintenance of GNSS networks that offer scientific-grade instrumentation, stable antenna monuments, and real-time data with low latency and few outages remains costly. However, the potential value of GNSS data from spatially dense arrays of low-cost sensors, used alone or in combination with observations from consumer-grade accelerometers, has been demonstrated (Minson *et al.*, 2015; Saunders *et al.*, 2016; Goldberg and Bock, 2017). Thus, in parallel with improvements to traditional geodetic-grade GNSS networks, the use of low-cost sensors merits further exploration to provide complementary data for strengthened monitoring and event response capabilities. Demonstrations of this approach include the deployment of instrument packages consisting of a micro-electro-mechanical systems (MEMS) accelerometer and on-site positioning module at 25 geodetic-grade GNSS stations in California (Saunders *et al.*, 2016), and a network combining smartphone MEMS accelerometers and external low-cost GPS chipsets for earthquake and tsunami warning in Chile (Brooks *et al.*, 2016).

GPS-acoustic (GPS-A) methods provide seafloor displacement measurements that illuminate subduction zone interseismic locking and slip on the megathrust (Bürgmann and Chadwell, 2014, and references therein). Such observations could clarify the up-dip limit of subduction zone locking, which in turn would reduce uncertainties in seismic hazard assessments. If continuously recorded, seafloor geodetic data would contribute to better understanding of the spatiotemporal evolution of SSEs. If available in real time, these data could substantially improve EEW for subduction zone events and could be invaluable for local tsunami warnings. Collaborative efforts are underway to further develop offshore monitoring in Cascadia (see Data and Resources) for research and event response applications. Objectives include expanding the GPS-A footprint and exploring feasible, cost-effective approaches to achieve real-time geodetic monitoring.

Analysis

ML and data-mining techniques have been used successfully to discover geophysical signals in large seismic datasets, offering new possibilities for the real-time detection, location, and characterization of earthquakes. Although ML has been proposed as a seismic detection tool since the 1990s (Wang and Teng, 1995), the expansion of seismic networks, combined with advances in instrument technology and data management over the past decade, has promoted active exploration of ways in which ML can improve early warning systems and reveal new empirical data-derived rules that have not yet been uncovered in traditional waveform analysis (Perol *et al.*, 2017; Kong *et al.*, 2018; Li *et al.*, 2018, Lomax *et al.*, 2019). The application of ML methods to geodetic datasets for transient detection, early warning, and eruption alerting is a natural extension of these ideas, with the potential to leverage the large amounts of data generated by continuous GNSS networks.

The availability of real-time GNSS data, along with observations from collocated seismic instruments and/or other geophysical sensors, will prompt further extension of new approaches to improve rapid assessment of earthquakes, eruptions, tsunamis, and their impacts. Although automated monitoring of GNSS data streams has been implemented in specific settings, for example, USGS volcano observatories, a more comprehensive system that combined anomaly detection and follow-on time-dependent (e.g., Johanson *et al.*, 2017) or physics-based (e.g., Anderson and Poland, 2016) modeling that would integrate multiple data types to inform ongoing event-response activities is an area of ongoing research and development.

In summary, these examples, although not intended to be an exhaustive list, exemplify the breadth of development that is currently underway. By capitalizing on these efforts, regional GNSS networks will support basic and applied research, monitoring, and the mitigation of losses from natural disasters.

Data and Resources

No data were used in this article. Data provided by individual networks may be accessed using the URLs in Tables 1 and 2. Some plots were made using the Generic Mapping Tools v.4.5.6 (www.soest.hawaii.edu/gmt, last accessed April 2019; Wessel and Smith, 1998). The offshore monitoring in Cascadia is available at http://cascadiaoffshore.org/index.html (last accessed April 2019). UNAVCO's geophysical event response page is available at https://www.unavco.org/projects/project-support/geophysical-event-response/geophysical-event-response.html (last accessed April 2019). IGSMail-466, 1994 Northridge earthquake is available at https://lists.igs.org/pipermail/igsmail/1994/001842.html (last accessed April 2019). The URLs of websites for the GNSS networks listed in Table 1 are as follows: Alaska Volcano Observatory (AVO): www.avo.alaska.edu, Bay Area Regional Deformation network (BARD): http://seismo.berkeley.edu/bard, California Volcano Observatory Long Valley network (CalVO): https://earthquake.usgs.gov/monitoring/gps/LongValley, Cascades Volcano Observatory (CVO): https://earthquake.usgs.gov/monitoring/gps/Pacific_Northwest, GPS Array for Mid-America (GAMA), http://www.ceri.memphis.edu/people/gps/, Hawaiian

Volcano Observatory (HVO): https://volcanoes.usgs.gov/observatories/hvo, Mobile Array of GPS for Nevada Transtension (MAGNET): http://geodesy.unr.edu/magnet.php, Northern California Global Navigation Satellite System (GNSS) Network (NCGN), https://earthquake.usgs.gov/monitoring/gps/SFBayArea, Network of the Americas (NOTA): http://www.unavco.org/, Pacific Northwest Geodetic Array (PANGA): https://www.geodesy.cwu.edu/, Puerto Rico Seismic Network (PRSN): http://redsismica.uprm.edu, Pacific GPS Facility (PGF): http://pgf.soest.hawaii.edu, Southern California GNSS Network (SCGN): https://earthquake.usgs.gov/monitoring/gps/Southern_California, Scripps Orbit and Permanent Array Center (SOPAC): http://sopac-csrc.ucsd.edu. The URLs for the data archives listed in Table 1 are as follows. UNAVCO: https://www.unavco.org/data/gps-gnss/data-access-methods/dai2/app/dai2.html. See https://www.unavco.org/data/gps-gnss/data-access-methods/data-access-methods.html for more information regarding how to access data archived at UNAVCO. Northern California Earthquake Data Center (NCEDC): http://ncedc.org/bard.overview.html. PANGA: https://www.geodesy.cwu.edu/data_ftp_pub/data; Pacific GPS Facility (PGF): http://pgf.soest.hawaii.edu/GPSDATA/public/data/cgps/. SOPAC: http://garner.ucsd.edu. For networks in Table 2 for which IP addresses are not listed, the following are the URLs with port numbers for connecting to real-time data streams. We also list URLs providing additional data access information as applicable. BARD and NCGN: http://tiburon.geo.berkeley.edu:2101/. See http://seismo.berkeley.edu/bard/realtime/ for data access information. California Real Time Network (CRTN): See http://sopac-csrc.ucsd.edu/index.php/crtn/ for data access instructions. NOTA: For PPP solutions: rtgpsout.unavco.org:/2110, for raw data in BINEX format: rtgpsout.unavco.org:/2105, for raw data in RTCM3.1 format: rtgpsout.unavco.org:/2101. See https://www.unavco.org/data/gps-gnss/real-time/real-time.html. PANGA: realtime.panga.cwu.edu:2101. See http://www.panga.cwu.edu/realtime/ for data access terms and conditions. PRSN: http://gps.uprm.edu:2101. SCGN: surfrider.gps.caltech.edu:/2101. Processed real-time streams for NCGN and SCGN can be viewed at https://escweb.wr.usgs.gov/share/highrate-gps/. Processed real-time streams for PANGA can be viewed at http://www.panga.org/realtime/data/. The GPS Data Performance Monitoring website discussed in Figure 9 is available at https://escweb.wr.usgs.gov/highrate-gps/. Unless otherwise noted, all websites were last accessed May 2019.

Acknowledgments

We thank Michael Floyd, Rebecca Kramer, Fred Pollitz, Evelyn Roeloffs, and an anonymous reviewer for thoughtful reviews that substantially improved the article. Any use of trade, firm, or product names is for descriptive purposes only and does not imply endorsement by the U.S. government.

References

Allen, R. M., and A. Ziv (2011). Application of real-time GPS to earthquake early warning, *Geophys. Res. Lett.* **38,** L16310, doi: 10.1029/2011GL047947.

Amos, C. B., P. Audet, W. C. Hammond, R. Burgmann, I. A. Johanson, and G. Blewitt (2014). Uplift and seismicity driven by groundwater depletion in central California, *Nature* **509,** 483–486, doi: 10.1038/nature13275.

Anderson, K. R., and M. P. Poland (2016). Bayesian estimation of magma supply, storage, and eruption rates using a multiphysical volcano model: Kīlauea Volcano, 2000–2012, *Earth Planet. Sci. Lett.* **447,** 161–171.

Argus, D. F., Y. Fu, and F. W. Landerer (2014). Seasonal variation in total water storage in California inferred from GPS observations of vertical land motion, *Geophys. Res. Lett.* **41,** 1971–1980, doi: 10.1002/2014GL059570.

Argus, D. F., F. W. Landerer, D. N. Wiese, H. R. Martens, Y. Fu, J. S. Famiglietti, B. F. Thomas, T. G. Farr, A. W. Moore, and M. M. Watkins (2017). Sustained water loss in California's mountain ranges during severe drought from 2012 to 2015 inferred from GPS, *J. Geophys. Res.* **122,** 10,559–10,585, doi: 10.1002/2017JB014424.

Bartlow, N. M., S. I. Miyazaki, A. M. Bradley, and P. Segall (2011). Space-time correlation of slip and tremor during the 2009 Cascadia slow slip event, *Geophys. Res. Lett.* **38,** L18309, doi: 10.1029/2011GL048714.

Battaglia, M., C. Roberts, and P. Segall (1999). Magma intrusion beneath Long Valley caldera confirmed by temporal changes in gravity, *Science* **285,** 2119–2122.

Bawden, G. W., W. Thatcher, R. S. Stein, K. W. Hudnut, and G. Peltzer (2001). Tectonic contraction across Los Angeles after removal of ground-water pumping effects, *Nature* **412,** 812–815.

Bevis, M., S. Businger, S. Chiswell, T. A. Herring, R. Anthes, C. Rocken, and R. H. Ware (1994). GPS meteorology: Mapping zenith wet delays onto precipitable water, *J. Appl. Meteor.* **33,** 379–386, doi: 10.1175/1520-0450(1994)033<0379:GMMZWD>2.0.CO;2.

Bird, P. (2009). Long-term fault slip rates, distributed deformation rates, and forecast of seismicity in the western United States from joint fitting of community geologic, geodetic, and stress direction data sets, *J. Geophys. Res.* **114,** no. B11403, doi: 10.1029/2009JB006317.

Blewitt, G., W. C. Hammond, and C. Kreemer (2018). Harnessing the GPS data explosion for interdisciplinary science, *Eos Trans. AGU* **99,** doi: 10.1029/2018EO104623.

Blewitt, G., M. B. Heflin, K. J. Hurst, D. C. Jefferson, F. H. Webb, and J. F. Zumberge (1993). Absolute far-field displacements from the 28 June 1992 Landers earthquake sequence, *Nature* **361,** 340–342.

Blewitt, G., C. Kreemer, and W. C. Hammond (2009). Geodetic observation of contemporary deformation in the northern Walker Lane: 1. Semipermanent GPS strategy, in *Late Cenozoic Structure and Evolution of the Great Basin-Sierra Nevada Transition*, J. S. Oldow and P. H. Cashman (Editors), Geol. Soc. Am. Spec. Pap. 447, 1–15, doi: 10.1130/2009.2447(01).

Blewitt, G., C. Kreemer, W. C. Hammond, H.-P. Plag, S. Stein, and E. Okal (2006). Rapid determination of earthquake magnitude using GPS for tsunami warning systems, *Geophys. Res. Lett.* **33,** L11309, doi: 10.1029/2006GL026145.

Blume, F., T. Herring, G. S. Mattioli, K. Feaux, C. Walls, K. E. Austin, and S. T. Dittmann (2017). Stability of GNSS monumentation: Analysis of co-located monuments in the UNAVCO Plate Boundary Observatory, *Abstract G14A-02 presented at 2017 AGU Fall Meeting*, New Orleans, Louisiana, 11–15 December.

Bock, Y., and D. Melgar (2016). Physical applications of GPS geodesy: A review, *Rep. Progr. Phys.* **79,** 106801, 119, doi: 10.1088/0034-4885/79/10/106801.

Bock, Y., D. C. Agnew, P. Fang, J. F. Genrich, B. H. Hager, T. A. Herring, K. W. Hudnut, R. W. King, S. Larsen, and J.-B. Minster (1993). Detection of crustal deformation from the Landers earthquake sequence using continuous geodetic measurements, *Nature* **361,** 337–340.

Bock, Y., S. Kedar, A. W. Moore, P. Fang, J. Geng, Z. Liu, D. Melgar, S. E. Owen, M. B. Squibb, and F. Webb (2016). Twenty-two years of combined GPS products for geophysical applications and a decade of seismogeodesy, in *International Symposium on Geodesy for Earthquake and Natural Hazards (GENAH)*, M. Hashimoto (Editor), International Association of Geodesy Symposia, Vol. 145, Springer, Cham, Switzerland, 49–54, doi: 10.1007/1345_2016_220.

Bock, Y., D. Melgar, and B. W. Crowell (2011). Real-time strong-motion broadband displacements from collocated GPS and accelerometers, *Bull. Seismol. Soc. Am.* **101,** 2904–2925, doi: 10.1785/0120110007.

Bock, Y., L. Prawirodirdjo, and T. I. Melbourne (2004). Detection of arbitrarily large dynamic ground motions with a dense high-rate GPS network, *Geophys. Res. Lett.* **31,** L06604, doi: 10.1029/2003GL019150.

Bock, Y., S. Wdowinski, P. Fang, J. Zhang, S. Williams, H. Johnson, J. Behr, J. Genrich, J. Dean, M. van Domselaar, *et al.* (1997). Southern California permanent GPS geodetic array: Continuous measurements of crustal deformation between the 1992 Landers and 1994 Northridge earthquakes, *J. Geophys. Res.* **102,** 18,013–18,033.

Borsa, A. A., D. C. Agnew, and D. R. Cayan (2014). Ongoing drought-induced uplift in the western United States, *Science* **345,** 1587–1590, doi: 10.1126/science.1260279.

Böse, M., D. E. Smith, C. Felizardo, M.-A. Meier, T. H. Heaton, and J. F. Clinton (2018). FinDer v.2: Improved real-time ground-motion predictions for M2–M9 with seismic finite-source characterization, *Geophys. J. Int.* **212,** 725–742, doi: 10.1093/gji/ggx430.

Braun, J. J., G. S. Mattioli, E. Calais, D. Carlson, T. Dixon, M. Jackson, R. Kursinski, H. Mora-Paez, M. M. Miller, R. Pandya, *et al.* (2012). Focused study of interweaving hazards across the Caribbean, *Eos Trans. AGU* **93,** 89, doi: 10.1029/2012EO090001.

Brooks, B. A., J. C. Baez, T. Ericksen, S. E. Barrientos, S. E. Minson, C. Duncan, C. Guillemot, D. Smith, M. Böse, E. Cochran, *et al.* (2016). Smartphone-based earthquake and tsunami early warning in Chile, *Abstract G31A-1045 presented at 2016 Fall Meeting AGU*, San Francisco, California, 12–16 December 2016.

Brooks, B. A., J. H. Foster, M. Bevis, L. N. Frazer, C. J. Wolfe, and M. Behn (2006). Periodic slow earthquakes on the flank of Kīlauea volcano, Hawai'i, *Earth Planet. Sci. Lett.* **246,** 207–216, doi: 10.1016/j.epsl.2006.03.035.

Bürgmann, R. (2018). The geophysics, geology and mechanics of slow fault slip, *Earth Planet. Sci. Lett.* **495,** 112–134.

Bürgmann, R., and D. Chadwell (2014). Seafloor geodesy, *Annu. Rev. Earth Planet. Sci.* **42,** 509–534, doi: 10.1146/annurev-earth-060313-054953.

Bürgmann, R., and W. Thatcher (2013). Space geodesy: A revolution in crustal deformation measurements of tectonic processes, *Geol. Soc. Am. Spec. Pap.* **500,** 397–430, doi: 10.1130/2013.2500(12).

Cabral-Cano, E., X. Pérez-Campos, B. Márquez-Azúa, M. A. Sergeeva, L. Salazar-Tlaczani, C. DeMets, D. Adams, J. Galetzka, K. Hodgkinson, K. Feaux, *et al.* (2018). TLALOCNet: A continuous GPS-Met backbone in Mexico for seismotectonic and atmospheric research, *Seismol. Res. Lett.* **89,** 373–381, doi: 10.1785/0220170190.

Cervelli, P., T. Fournier, J. T. Freymueller, and J. Power (2006). Ground deformation associated with the precursory unrest and early phases of the January 2006 eruption of Augustine volcano, Alaska, *Geophys. Res. Lett.* **33,** L18304, doi: 10.1029/2006GL027219.

Cervelli, P., T. J. Fournier, J. T. Freymueller, J. A. Power, M. Lisowski, and B. A. Pauk (2010). Geodetic constraints on magma movement and withdrawal during the 2006 eruption of Augustine volcano, in *The 2006 Eruption of Augustine Volcano, Alaska*, J. A. Power, M. L. Coombs, and J. T. Freymueller (Editors), U.S. Geol. Surv. Profess. Pap. 1769, U.S. Geological Survey, Reston, Virginia.

Cervelli, P., P. Segall, K. Johnson, M. Lisowski, and A. Miklius (2002). Sudden aseismic fault slip on the south flank of Kīlauea volcano, *Nature* **415,** 1014–1018.

Chang, W.-L., R. B. Smith, J. Farrell, and C. M. Puskas (2010). An extraordinary episode of Yellowstone caldera uplift, 2004–2010, from GPS and InSAR observations, *Geophys. Res. Lett.* **37,** L23302, doi: 10.1029/2010GL045451.

Crowell, B. W., D. Melgar, Y. Bock, J. S. Haase, and J. Geng (2013). Earthquake magnitude scaling using seismogeodetic data, *Geophys. Res. Lett.* **40,** 6089–6094, doi: 10.1002/2013GL058391.

Crowell, B. W., D. A. Schmidt, P. Bodin, J. E. Vidale, J. Gomberg, J. R. Hartog, V. C. Kress, T. I. Melbourne, M. Santillan, S. E. Minson, and D. G. Jamison (2016). Demonstration of the Cascadia G-FAST geodetic earthquake early warning system for the Nisqually, Washington, earthquake, *Seismol. Res. Lett.* **87,** 930–943, doi: 10.1785/0220150255.

Davis, J. L., B. P. Wernicke, and M. E. Tamisiea (2012). On seasonal signals in geodetic time series, *J. Geophys. Res.* **117,** no. B01403, doi: 10.1029/2011JB008690.

Dixon, T. H. (1991). An introduction to the global positioning system and some geological applications, *Rev. Geophys.* **29,** 249–276, doi: 10.1029/91RG00152.

Dragert, H., and R. D. Hyndman (1995). Continuous GPS monitoring of elastic strain in the Northern Cascadia subduction zone, *Geophys. Res. Lett.* **22,** 755–758, doi: 10.1029/95GL00469.

Dragert, H., K. Wang, and T. S. James (2001). A silent slip event on the deeper Cascadia subduction interface, *Science* **292,** 1525–1528.

Farrell, J., R. B. Smith, T. Taira, W.-L. Chang, and C. M. Puskas (2010). Dynamics and rapid migration of the energetic 2008–2009 Yellowstone Lake earthquake swarm, *Geophys. Res. Lett.* **37,** L19305, doi: 10.1029/2010GL044605.

Flesch, L., W. E. Holt, A. J. Haines, L. Wen, and B. Shen-Tu (2007). The dynamics of western North America: Stress magnitudes and the relative role of gravitational potential energy, plate interaction at the boundary and basal tractions, *Geophys. J. Int.* **169,** 866–896.

Foster, J. (2015). GPS and Surveying, in *Handbook of Sea-Level Research*, I. Shennan, A. J. Long, and B. P. Horton (Editors), John Wiley & Sons, Ltd., Chichester, United Kingdom, 157–170, doi: 10.1002/9781118452547.ch10.

Foster, J., and M. Bevis (2003). Lognormal distribution of precipitable water in Hawai'i, *Geochem. Geophys. Geosys.* **4,** no. 7, 1065, doi: 10.1029/2002GC000478.

Foster, J., M. Bevis, Y.-L. Chen, S. Businger, and Y. Zhang (2003). The Ka' storm (November 2000): Imaging precipitable water using GPS, *J. Geophys. Res.* **108,** no. D18, 4585, doi: 10.1029/2003JD003413.

Fournier, T., J. T. Freymueller, and P. Cervelli (2009). Tracking magma volume recovery at Okmok Volcano using GPS and an Unscented Kalman Filter, *J. Geophys. Res.* **114,** no. B02405, doi: 10.1029/2008JB005837.

Fu, Y., D. F. Argus, and F. W. Landerer (2015). GPS as an independent measurement to estimate terrestrial water storage variations in

Washington and Oregon, *J. Geophys. Res.* **120,** 552–566, doi: 10.1002/2014JB011415.

Fu, Y., Z. Liu, and J. T. Freymueller (2015). Spatiotemporal variations of the slow slip event between 2008 and 2013 in the southcentral Alaska subduction zone, *Geochem. Geophys. Geosys.* **16,** 2450–2461, doi: 10.1002/2015GC005904.

Geng, J., Y. Pan, X. Li, J. Guo, J. Liu, X. Chen, and Y. Zhang (2018). Noise characteristics of high-rate multi-GNSS for subdaily crustal deformation monitoring, *J. Geophys. Res.* **123,** 1987–2002, doi: 10.1002/2018JB015527.

Given, D. D., R. M. Allen, A. S. Baltay, P. Bodin, E. S. Cochran, K. Creager, L. S. Gee, E. Hauksson, T. H. Heaton, M. Hellweg, *et al.* (2018). Revised technical implementation plan for the ShakeAlert system—An earthquake early warning system for the West Coast of the United States, *U.S. Geol. Surv. Open-File Rept. 2018-1155*, 42, doi: 10.3133/ofr20181155.

Goldberg, D. E., and Y. Bock (2017). Self-contained local broadband seismogeodetic early warning system: Detection and location, *J. Geophys. Res.* **122,** 3197–3220, doi: 10.1002/2016JB013766.

Goldberg, D. E., D. Melgar, Y. Bock, and R. M. Allen (2018). Geodetic observations of weak determinism in rupture evolution of large earthquakes, *J. Geophys. Res.* **123,** 9950–9962, doi: 10.1029/2018JB015962.

Grapenthin, R., I. A. Johanson, and R. M. Allen (2014). Operational real-time GPS-enhanced earthquake early warning, *J. Geophys. Res.* **119,** 7944–7965, doi: 10.1002/2014JB011400.

Grapenthin, R., M. West, and J. Freymueller (2017). The utility of GNSS for earthquake early warning in regions with sparse seismic networks, *Bull. Seismol. Soc. Am.* **107,** 1883–1890, doi: 10.1785/0120160317.

Hernández, F. J., and F. A. Martínez (2018). A new library for interfacing Python with Earthworm: PyEarthWorm, *Abstract NS53A-0564 presented at 2018 Fall Meeting, AGU*, Washington, D.C., 10–14 December 2018.

Herring, T. A., R. W. King, M. A. Floyd, and S. C. McClusky (2015). *Introduction to GAMIT/GLOBK, Release 10.6*, Massachusetts Institute of Technology, Cambridge, Massachusetts.

Herring, T. A., T. I. Melbourne, M. H. Murray, M. A. Floyd, W. M. Szeliga, R. W. King, D. A. Phillips, C. M. Puskas, M. Santillan, and L. Wang (2016). Plate boundary observatory and related networks: GPS data analysis methods and geodetic products, *Rev. Geophys.* **54,** 759–808, doi: 10.1002/2016RG000529.

Hill, E. M., J. L. Davis, P. Elósegui, B. P. Wernicke, E. Malikowski, and N. A. Niemi (2009). Characterization of site specific GPS errors using a short-baseline network of braced monuments at Yucca Mountain, southern Nevada, *J. Geophys. Res.* **114,** no. B11402, doi: 10.1029/2008JB006027.

Hoshiba, M., and T. Ozaki (2014). Earthquake early warning and tsunami warning of the Japan Meteorological Agency, and their performance in the 2011 off the Pacific Coast of Tohoku earthquake (M 9.0), in *Early Warning for Geological Disasters*, F. Wenzel and J. Zschau (Editors), Springer, Berlin, Germany, 1–28,.

Hudnut, K. W., Y. Bock, J. E. Galetzka, F. H. Webb, and W. H. Young (2002). The Southern California integrated GPS network (SCIGN), in *Seismotectonics in Convergent Plate Boundary*, Y. Fujinawa and A. Yoshida (Editors), 167–189, TERRAPUB, Tokyo, Japan.

Hudnut, K. W., Z. Shen, M. Murray, S. McClusky, R. King, T. Herring, B. Hager, Y. Feng, P. Fang, A. Donnellan, and Y. Bock (1996). Co-seismic displacements of the 1994 Northridge, California, earthquake, *Bull. Seismol. Soc. Am.* **86,** S19–S36.

Johanson, I. A., A. Miklius, P. Okubo, and E. K. Montgomery-Brown (2017). Variability of the 2014-present inflation source at Mauna Loa volcano revealed using time-dependent modeling, *Abstract V34C-03 presented at 2017 AGU Fall Meeting*, New Orleans, Louisiana, 11–15 December.

Johnson, C. W., Y. Fu, and R. Bürgmann (2017). Stress models of the annual hydrospheric, atmospheric, thermal, and tidal loading cycles on California faults: Perturbation of background stress and changes in seismicity, *J. Geophys. Res.* **122,** 10,605–10,625, doi: 10.1002/2017JB014778.

King, N. E., D. Argus, J. Langbein, D. C. Agnew, G. Bawden, R. S. Dollar, Z. Liu, D. Galloway, E. Reichard, A. Yong, *et al.* (2007). Space geodetic observation of expansion of the San Gabriel Valley, California, aquifer system, during heavy rainfall in winter 2004-2005, *J. Geophys. Res.* **112,** no. B03409, doi: 10.1029/2006JB004448.

Komjathy, A., Y.-M. Yang, X. Meng, O. Verkhoglyadova, A. J. Mannucci, and R. B. Langley (2016). Review and perspectives: Understanding natural-hazards-generated ionospheric perturbations using GPS measurements and coupled modeling, *Radio Sci.* **51,** 951–961, doi: 10.1002/2015RS005910.

Kong, Q., A. Inbal, R. M. Allen, Q. Lv, and A. Puder (2018). Machine learning aspects of the MyShake global smartphone seismic network, *Seismol. Res. Lett.* **90,** 546–552, doi: 10.1785/0220180309.

Kraner, M. L., W. E. Holt, and A. A. Borsa (2018). Seasonal nontectonic loading inferred from cGPS as a potential trigger for the M6.0 South Napa earthquake, *J. Geophys. Res.* **123,** 5300–5322, doi: 10.1029/2017JB015420.

Kreemer, C., and W. C. Hammond (2007). Geodetic constraints on areal-changes in the Pacific-North America plate boundary zone: What controls Basin and Range extension?, *Geology* **35,** 943–947, doi: 10.1130/G23868A.1.

Kreemer, C., and I. Zaliapin (2018). Spatiotemporal correlation between seasonal variations in seismicity and horizontal dilatational strain in California, *Geophys. Res. Lett.* **45,** 9559–9568, doi: 10.1029/2018GL079536.

Kreemer, C., W. C. Hammond, G. Blewitt, A. Holland, and R. A. Bennett (2012). A geodetic strain rate model for the southwestern United States, scale 1:1,500,000, *Nevada Bureau of Mines and Geology Publication M178*, available at http://pubs.nbmg.unr.edu/Geod-strain-rate-full-size-p/m178.htm (last accessed August 2019).

Langbein, J. (2008). Noise in GPS displacement measurements from Southern California and Southern Nevada, *J. Geophys. Res.* **113,** no. B05405, doi: 10.1029/2007JB005247.

Langbein, J., and Y. Bock (2004). High-rate real-time GPS network at Parkfield: Utility for detecting fault slip and seismic displacements, *Geophys. Res. Lett.* **31,** L15S20, doi: 10.1029/2003GL019408.

Langbein, J., and J. L. Svarc (2019). Evaluation of temporally correlated noise in Global Navigation Satellite System time series: Geodetic monument performance, *J. Geophys. Res.* **124,** 925–942, doi: 10.1029/2018JB016783.

Langbein, J., J. R. Murray, and H. A. Snyder (2006). Coseismic and initial postseismic deformation from the 2004 Parkfield, California, earthquake, observed by Global Positioning System, electronic distance meter, creepmeters, and borehole strainmeters, *Bull. Seismol. Soc. Am.* **96,** S304–S320, doi: 10.1785/0120050823.

Larson, K. M. (2016). GPS interferometric reflectometry: Applications to surface soil moisture, snow depth, and vegetation water content in the western United States, *WIREs Water* **3,** 775–787, doi: 10.1002/wat2.1167.

Larson, K. M., P. Bodin, and J. Gomberg (2003). Using 1-Hz GPS data to measure deformations caused by the Denali Fault earthquake, *Science* **300,** 1421–1424.

Larson, K. M., R. D. Ray, F. G. Nievinski, and J. T. Freymueller (2013). The accidental tide gauge: A GPS reflection case study from Kachemak Bay, Alaska, *IEEE Geosci. Rem. Sens. Lett.* **10,** 1200–1204, doi: 10.1109/LGRS.2012.2236075.

Li, S., J. Freymueller, and R. McCaffrey (2016). Slow slip events and time-dependent variations in locking beneath Lower Cook Inlet of the Alaska-Aleutian subduction zone, *J. Geophys. Res.* **121,** 1060–1079, doi: 10.1002/2015JB012491.

Li, Z., M.-A. Meier, E. Hauksson, Z. Zhan, and J. Andrews (2018). Machine learning seismic wave discrimination: Application to earthquake early warning, *Geophys. Res. Lett.* **45,** 4773–4779, doi: 10.1029/2018GL077870.

Lisowski, M. D., D. Dzurisin, R. P. Denlinger, and E. Y. Iwatsubo (2008). Analysis of GPS-measured deformation associated with the 2004–2006 dome-building eruption of Mount St. Helens, Washington, in *A Volcano Rekindled: The Renewed Eruption of Mount St. Helens, 2004–2006*, D. R. Sherrod, W. E. Scott, and P. H. Stauffer (Editors), U.S. Geol. Surv. Profess. Pap. 1750, U.S. Geological Survey, Reston, Virginia, 856 pp.

Lomax, A., A. Michelini, and D. Jozinović (2019). An investigation of rapid earthquake characterization using single-station waveforms and a convolutional neural network, *Seismol. Res. Lett.* **90,** 517–529, doi: 10.1785/0220180311.

López, A. M., F. J. Hernández, and E. A. Vanacore (2018). Ingesting real-time GNSS positions, displacements and velocities into earthworm for potential usage in earthquake and tsunami early warning systems, *Abstract IN43D-0924 presented at 2018 Fall Meeting, AGU*, Washington, D.C., 10–14 December 2018.

Mattioli, G. S., and P. E. Jansma (2007). Evaluation of monument stability and noise associated with campaign and continuous GPS geodesy in the New Madrid seismic zone and other areas of unconsolidated sediment, *Final Tech. Rept. NEHRP 02HQGR0107*, G. Mattioli (Editor), 19 pp., available at https://earthquake.usgs.gov/cfusion/external_grants/reports/02HQGR0107.pdf (last accessed August 2019).

Mattioli, G. S., P. E. Jansma, J. Davis, and R. Smalley (2007). Experimental investigation of monument stability in the New Madrid seismic zone, *EarthScope Annual Meeting*, Monterey, California, 27–30 March 2007.

Melgar, D., and Y. Bock (2015). Kinematic earthquake source inversion and tsunami runup prediction with regional geophysical data, *J. Geophys. Res.* **120,** 3324–3349, doi: 10.1002/2014JB011832.

Melgar, D., and G. P. Hayes (2017). Systematic observations of the slip pulse properties of large earthquake ruptures, *Geophys. Res. Lett.* **44,** 9691–9698, doi: 10.1002/2017GL074916.

Melgar, D., R. M. Allen, S. Riquelme, J. Geng, F. Bravo, J. C. Baez, H. Parra, S. Barrientos, P. Fang, Y. Bock, *et al.* (2016). Local tsunami warnings: Perspectives from recent large events, *Geophys. Res. Lett.* **43,** 1109–1117, doi: 10.1002/2015GL067100.

Melgar, D., B. W. Crowell, J. Geng, R. M. Allen, Y. Bock, S. Riquelme, E. M. Hill, M. Protti, and A. Ganas (2015). Earthquake magnitude calculation without saturation from the scaling of peak ground displacement, *Geophys. Res. Lett.* **42,** 5197–5205, doi: 10.1002/2015GL064278.

Miller, M. M., T. Melbourne, D. J. Johnson, and W. Q. Sumner (2002). Periodic slow earthquakes from the Cascadia Subduction Zone, *Science* **295,** 2423.

Minson, S. E., B. A. Brooks, C. L. Glennie, J. R. Murray, J. O. Langbein, S. E. Owen, T. H. Heaton, R. A. Iannucci, and D. L. Hauser (2015). Crowdsourced earthquake early warning, *Sci. Adv.* **1,** e1500036, doi: 10.1126/sciadv.1500036.

Minson, S. E., J. R. Murray, J. O. Langbein, and J. S. Gomberg (2014). Real-time inversions for finite fault slip models and rupture geometry based on high-rate GPS data, *J. Geophys. Res.* **119,** doi: 10.1002/2013JB010622.

Montgomery-Brown, E. K., P. Segall, and A. Miklius (2009). Kīlauea slow slip events: Identification, source inversions, and relation to seismicity, *J. Geophys. Res.* **114,** no. B00A03, doi: 10.1029/2008JB006074.

Montgomery-Brown, E. K., C. W. Wicks, P. F. Cervelli, J. O. Langbein, J. L. Svarc, D. R. Shelly, D. P. Hill, and M. Lisowski (2015). Renewed inflation of Long Valley Caldera, California (2011 to 2014), *Geophys. Res. Lett.* **42,** 5250–5257, doi: 10.1002/2015GL064338.

Moore, A. W., I. J. Small, S. I. Gutman, Y. Bock, J. L. Dumas, P. Fang, J. S. Haase, M. E. Jackson, and J. L. Laber (2015). National weather service forecasters use GPS precipitable water vapor for enhanced situational awareness during the southern California summer monsoon, *Bull. Am. Meteor. Soc.* **96,** 1867–1877, doi: 10.1175/BAMS-D-14-00095.1.

Murray, J. R., and J. L. Svarc (2017). Global Positioning System data collection, processing, and analysis conducted by the U.S. Geological Survey Earthquake Hazards Program, *Seismol. Res. Lett.* **88,** 916–925, doi: 10.1785/0220160204.

Murray, J. R., B. W. Crowell, R. Grapenthin, K. Hodgkinson, J. O. Langbein, T. Melbourne, D. Melgar, S. E. Minson, and D. A. Schmidt (2018). Development of a geodetic component for the U.S. west coast earthquake early warning system, *Seismol. Res. Lett.* **89,** 2322–2336, doi: 10.1785/0220180162.

Neal, C. A., S. R. Brantley, L. Antolik, J. L. Babb, M. Burgess, K. Calles, M. Cappos, J. C. Chang, S. Conway, L. Desmither, *et al.* (2019). The 2018 rift eruption and summit collapse of Kīlauea Volcano, *Science* **363,** 367–374.

Nikolaidis, R. M., Y. Bock, P. J. de Jonge, P. Shearer, D. C. Agnew, and M. Van Domselaar (2001). Seismic wave observations with the Global Positioning System, *J. Geophys. Res.* **106,** 21,897–21,916.

Occhipinti, G., L. Rolland, P. Lognonné, and S. Watada (2013). From Sumatra 2004 to Tohoku–Oki 2011: The systematic GPS detection of the ionospheric signature induced by tsunamigenic earthquakes, *J. Geophys. Res.* **118,** 3626–3636, doi: 10.1002/jgra.50322.

Ohta, Y., J. T. Freymueller, S. Hreinsdóttir, and H. Suito (2006). A large slow slip event and the depth of the seismogenic zone in the south central Alaska subduction zone, *Earth Planet. Sci. Lett.* **247,** 108–116.

Parsons, T., and W. Thatcher (2011). Diffuse Pacific–North American plate boundary: 1000 km of dextral shear inferred from modeling geodetic data, *Geology* **39,** 943–946, doi: 10.1130/G32176.1.

Parsons, T., K. M. Johnson, P. Bird, J. Bormann, T. E. Dawson, E. H. Field, W. C. Hammond, T. A. Herring, R. McCaffrey, Z.-K. Shen, *et al.* (2013). Deformation models for UCERF3, in *Uniform*

California Earthquake Rupture Forecast, Version 3 (UCERF3)—The Time-Independent Model, E. H. Field, *et al.*, U.S. Geol. Surv. Open-File Rept. 2013-1165, California Geol. Surv. Spec. Rept. 228, and Southern California Earthquake Center Publication 1792, U.S. Geological Survey, Reston, Virginia, 97 pp.

Peng, Z., and J. Gomberg (2010). An integrated perspective of the continuum between earthquakes and slow-slip phenomena, *Nature Geosci.* **3,** 599–607.

Perol, T., M. Gharbi, and M. Denolle (2017). Convolutional neural network for earthquake detection and location, *Sci. Adv.* **4,** e1700578, doi: 10.1126/sciadv.1700578.

Petersen, M. D., Y. Zeng, K. M. Haller, R. McCaffrey, W. C. Hammond, P. Bird, M Moschetti, Z. Shen, J. Bormann, and W. Thatcher (2014). Geodesy- and geology-based slip-rate models for the Western United States (excluding California) national seismic hazard maps, *U.S. Geol. Surv. Open-File Rept. 2013-1293*, 80 pp., doi: 10.3133/ofr20131293.

Poland, M. P., M. Lisowski, D. Dzurisin, R. Kramer, M. McLay, and B. Pauk (2017). Volcano geodesy in the Cascade Arc, USA, *Bull. Volcanol.* **79,** 59, doi: 10.1007/s00445-017-1140-x.

Pollitz, F. F., P. McCrory, J. Svarc, and J. Murray (2008). Dislocation models of interseismic deformation in the western United States, *J. Geophys. Res.* **113,** no. B04413, doi: 10.1029/2007JB005174.

Pritchard, M., S. Owen, S. Anandakrishnan, W. Holt, R. Bennett, P. La Femina, P. Jansma, I. MacGregor, C. Raymond, S. Schwartz, *et al.* (2012). Open access to geophysical data sets requires community responsibility, *Eos Trans. AGU* **93,** 243, doi: 10.1029/2012EO260006.

Radhakrishna, B., F. Fabry, J. J. Braun, and T. Van Hove (2015). Precipitable water from GPS over the continental United States: Diurnal cycle, intercomparisons with NARR, and link with convective initiation, *J. Climate* **28,** 2584–2599, doi: 10.1175/JCLI-D-14-00366.1.

Rhie, J., D. S. Dreger, M. Murray, and N. Houlié (2009). Peak ground velocity ShakeMaps derived from geodetic slip models, *Geophys. J. Int.* **179,** 1105–1112, doi: 10.1111/j.1365-246X.2009.04327.x.

Rogers, G., and H. Dragert (2003). Episodic tremor and slip on the Cascadia subduction zone: The chatter of silent slip, *Science* **300,** 1942–1943.

Ruhl, C. J., D. Melgar, R. Grapenthin, and R. M. Allen (2017). The value of real-time GNSS to earthquake early warning, *Geophys. Res. Lett.* **44,** 8311–8319, doi: 10.1002/2017GL074502.

Saunders, J. K., D. E. Goldberg, J. S. Haase, Y. Bock, D. G. Offield, D. Melgar, J. Restrepo, R. B. Fleischman, A. Nema, J. Geng, *et al.* (2016). Seismogeodesy using GPS and low-cost MEMS accelerometers: Perspectives for earthquake early warning and rapid response, *Bull. Seismol. Soc. Am.* **106,** 2469–2489, doi: 10.1785/0120160062.

Savastano, G., A. Komjathy, O. Verkhoglyadova, A. Mazzoni, M. Crespi, Y. Wei, and A. J. Mannucci (2017). Real-time detection of tsunami ionospheric disturbances with a stand-alone GNSS receiver: A preliminary feasibility demonstration, *Sci. Rep.* **7,** 46607, doi: 10.1038/srep46607.

Schwartz, S. Y., and J. M. Rokosky (2007). Slow slip events and seismic tremor at circum-Pacific subduction zones, *Rev. Geophys.* **45,** doi: 10.1029/2006RG000208.

Segall, P., and J. L. Davis (1997). GPS Applications for geodynamics and earthquake studies, *Annu. Rev. Earth Planet. Sci.* **25,** 301–336.

Shen, Z.-K., D. D. Jackson, Y. Feng, M. Cline, M. Kim, P. Fang, and Y. Bock (1994). Postseismic deformation following the Landers earthquake, California, 28 June 1992, *Bull. Seismol. Soc. Am.* **84,** 780–791.

Smith, T. L., S. G. Benjamin, S. I. Gutman, and S. Sahm (2007). Short-range forecast impact from assimilation of GPS-IPW observations into the rapid update cycle, *Mon. Weather Rev.* **135,** 2914–2930, doi: 10.1175/MWR3436.1.

Stough, T., and D. S. Green (2016). Collaborative demonstration for GNSS-augmented tsunami early warnings, *Abstract G44A-03 presented at 2016 AGU Fall Meeting*, San Francisco, California, 12–16 December.

Szeliga, W., T. Melbourne, M. Santillan, and M. Miller (2008). GPS constraints on 34 slow slip events within the Cascadia subduction zone, 1997–2005, *J. Geophys. Res.* **113,** no. B04404, doi: 10.1029/2007JB004948.

U.S. Geological Survey (USGS) (2017). Advanced National Seismic System—Current status, development opportunities, and priorities for 2017–2027, *U.S. Geol. Surv. Circ. 1429*, 32, doi: 10.3133/cir1429.

Wang, J., and T.-L. Teng (1995). Artificial neural network-based seismic detector, *Bull. Seismol. Soc. Am.* **85,** 308–319.

Wang, M., J. Wang, Y. Bock, H. Liang, D. Dong, and P. Fang (2019). Dynamic mapping of the movement of landfalling atmospheric rivers over southern California with GPS data, *Geophys. Res. Lett.* **46,** doi: 10.1029/2018GL081318.

Weber, G., D. Dettmering, H. Gebhard, and R. Kalafus (2005). Networked transport of RTCM via Internet Protocol (Ntrip)—IP-streaming for real-time GNSS applications, *ION GNSS 18th International Technical Meeting of the Satellite Division*, Long Beach, California, 13–16 September 2005, 2243–2247.

Wessel, P., and W. H. F. Smith (1998). New, improved version of the generic mapping tools released, *EOS Trans. AGU* 79, 579, doi: 10.1029/98EO00426.

Williams, M. L., K. M. Fischer, J. T. Freymueller, B. Tikoff, A. M. Tréhu, *et al.* (2010). *Unlocking the Secrets of the North American Continent: An EarthScope Science Plan for 2010–2020*, February, 2010, 78 pp; available http://www.earthscope.org/sites/default/files/escope/assets/uploads/pages/es_sci_plan_hi.pdf (last accessed August 2019).

Zietlow, D., C. Molnar, C. Meertens, D. Phillips, B. Bartel, and D. Ertz (2016). Geodetic data via web services: Standardizing access, expanding accessibility, and promoting discovery, *Abstract IN53C-1892 presented at 2016 AGU Fall Meeting*, San Francisco, California, 12–16 December.

Zumberge, J. F., M. B. Heflin, D. C. Jefferson, M. M. Watkins, and F. H. Webb (1997). Precise point positioning for the efficient and robust analysis of GPS data from large networks, *J. Geophys. Res.* **102,** 5005–5017, doi: 10.1029/96JB03860.

Manuscript received 13 May 2019
Published online 4 September 2019